HHS Public Access

Author manuscript

Cell Rep. Author manuscript; available in PMC 2024 May 07.

Published in final edited form as:

Cell Rep. 2024 March 26; 43(3): 113881. doi:10.1016/j.celrep.2024.113881.

Liver-derived plasminogen mediates muscle stem cell expansion during caloric restriction through the plasminogen receptor Plg-R_{KT}

Akshay Bareja[1,2], **David E. Lee**[1,2], **Tricia Ho**[8], **Greg Waitt**[8], **Lauren H. McKay**[2,17], **Sarah A. Hannou**[2], **Melissa C. Orenduff**[2], **Kristen M. McGreevy**[4], **Alexandra Binder**[5,6], **Calen P. Ryan**[9], **Erik J. Soderblom**[8], **Daniel W. Belsky**[9], **Luigi Ferrucci**[11], **Jayanta Kumar Das**[11], **Nirad Banskota**[12], **Virginia B. Kraus**[1,2,3], **Janet L. Huebner**[2], **William E. Kraus**[1,2,3], **Kim M. Huffman**[1,2,3], **Gurpreet S. Baht**[2,3,7], **Steve Horvath**[10,13], **Robert J. Parmer**[14,15], **Lindsey A. Miles**[16], **James P. White**[1,2,3,18,*]

[1]Department of Medicine, Duke University School of Medicine, Durham, NC 27710, USA

[2]Duke Molecular Physiology Institute, Duke University School of Medicine, Durham, NC 27701, USA

[3]Duke Center for the Study of Aging and Human Development, Duke University School of Medicine, Durham, NC 27701, USA

[4]Department of Biostatistics, UCLA Fielding School of Public Health, Los Angeles, CA 90095, USA

[5]Population Sciences in the Pacific Program (Cancer Epidemiology), University of Hawaii Cancer Center, University of Hawaii at Manoa, Honolulu, HI 96813, USA

[6]Department of Epidemiology, UCLA Fielding School of Public Health, Los Angeles, CA 90095, USA

[7]Department of Orthopedic Surgery, Duke University School of Medicine, Durham, NC 27701, USA

[8]Proteomics and Metabolomics Core Facility, Duke University School of Medicine, Durham, NC, USA

[9]Columbia University Mailman School of Public Health, New York, NY, USA

[*]Correspondence: james.white@duke.edu.

AUTHOR CONTRIBUTIONS

A. Bareja and J.P.W. designed the studies and carried out experiments with assistance from D.E.L., T.H., G.W., L.H.M., S.A.H., M.C.O., E.J.S., and J.L.H. Human epigenetic experiments and analyses were performed by K.M.M., A. Binder, C.P.R., D.W.B., and S.H. Data analysis and interpretation was assisted by D.W.B., W.E.K., K.M.H., V.B.K., G.S.B., R.J.P., and L.A.M. L.F., J.K.D., and N.B. generated the human muscle RNA-seq data. A. Bareja and J.P.W. wrote the paper. J.P.W. provided guidance and oversight throughout the project. All authors reviewed and approved the final version of the manuscript.

SUPPLEMENTAL INFORMATION

Supplemental information can be found online at https://doi.org/10.1016/j.celrep.2024.113881.

DECLARATION OF INTERESTS

The authors declare no competing interests.

[10]Department of Human Genetics, David Geffen School of Medicine, University of California, Los Angeles, Los Angeles, CA 90095, USA

[11]Longitudinal Studies Section, Translation Gerontology Branch, National Institute on Aging, National Institutes of Health, Baltimore, MD, USA

[12]Computational Biology and Genomics Core, National Institute on Aging, National Institutes of Health, Baltimore, MD, USA

[13]Altos Labs, San Diego, CA, USA

[14]Department of Medicine, Veterans Administration San Diego Healthcare System, San Diego, CA, USA

[15]Department of Medicine, University of California San Diego, La Jolla, CA, USA

[16]Department of Molecular Medicine, Scripps Research, La Jolla, CA 92037, USA

[17]Division of Oral and Craniofacial Health Sciences, Adams School of Dentistry, University of Chapel Hill, Chapel Hill, NC, USA

[18]Lead contact

SUMMARY

An intriguing effect of short-term caloric restriction (CR) is the expansion of certain stem cell populations, including muscle stem cells (satellite cells), which facilitate an accelerated regenerative program after injury. Here, we utilized the *MetRS*^{L274G} (MetRS) transgenic mouse to identify liver-secreted plasminogen as a candidate for regulating satellite cell expansion during short-term CR. Knockdown of circulating plasminogen prevents satellite cell expansion during short-term CR. Furthermore, loss of the plasminogen receptor KT (Plg-R_{KT}) is also sufficient to prevent CR-related satellite cell expansion, consistent with direct signaling of plasminogen through the plasminogen receptor Plg-R_{KT}/ERK kinase to promote proliferation of satellite cells. Importantly, we are able to replicate many of these findings in human participants from the CALERIE trial. Our results demonstrate that CR enhances liver protein secretion of plasminogen, which signals directly to the muscle satellite cell through Plg-R_{KT} to promote proliferation and subsequent muscle resilience during CR.

Graphical abstract

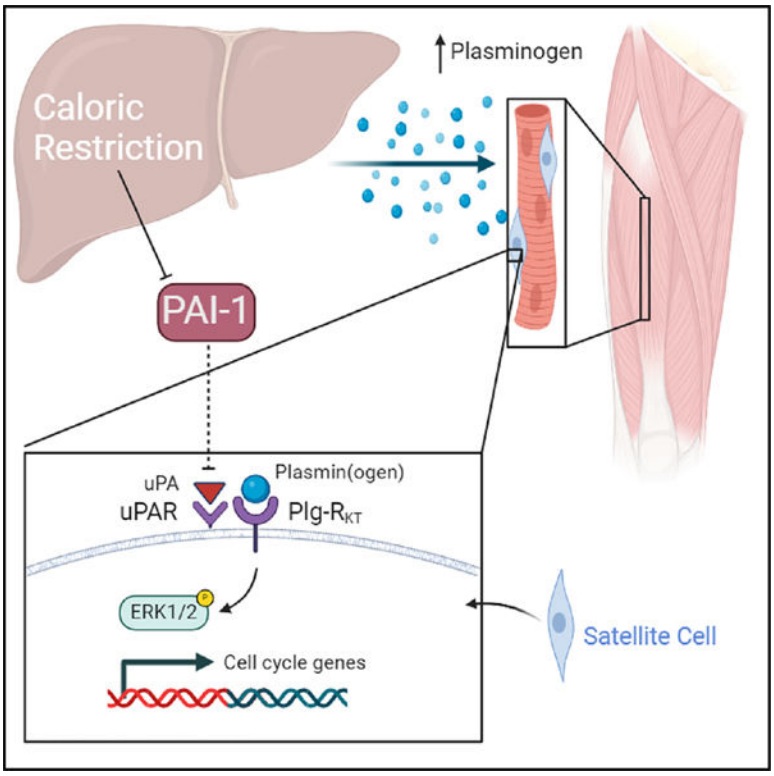

In brief

Short-term caloric restriction (CR) has been shown to expand the muscle satellite cell pool and accelerate the early phase of muscle regeneration. Bareja et al. report robust changes in the liver-derived plasma proteome during CR and identify plasminogen as a contributing factor to the satellite cell expansion, signaling through Plg-R$_{KT}$.

INTRODUCTION

The beneficial effects of caloric restriction (CR) are exemplified by reproducible lifespan and health span extension across a myriad of species, from *C. elegans* to non-human primates.[1] CR has known benefits for metabolism and/or function in several tissues, including muscle,[2,3] brain,[4], liver,[5] and hematopoietic[6] and cardiac[7] tissues. Beyond these effects, CR enhances tissue resilience, especially in muscle tissues.[8,9] In rodent skeletal muscle, CR promotes expansion of muscle stem cells, referred to as satellite cells, after short-term (3-month) CR.[8,10,11] There are emerging hypotheses suggesting that the beneficial effects of CR are mediated via the release of therapeutic secretory factors. However, the majority of studies examining the mechanism(s) of CR action have focused on intracellular effects, such as enhanced autophagy and mitochondrial function.[8,11,12] Further investigation is warranted to determine the systemic/extracellular effects of CR and how this could alter stem cell function and tissue resilience.

The recently developed *MetRS*^{L274G} transgenic mouse[13,14] allows for the generation of labeled proteins and can be made tissue specific via the Cre/*loxP* system. This technology

can be leveraged to identify secreted plasma proteins derived from their respective tissues using mass spectrometry-based proteomics. The *MetRS*^{L274G} model has been used previously to identify muscle and brain-derived proteins.[13,15] This proteomics technology has not been used to identify CR-responsive proteins and secretion patterns for individual tissues.

Over the last few decades, multiple studies have shown that plasminogen and/or plasmin play a role in multiple processes beyond their canonical role in hemostasis, including tissue resilience and regeneration. Plasminogen-deficient mice show regenerative perturbations across several tissues, including skeletal muscle,[16] liver,[17,18] and skin.[19,20] More specifically, plasminogen regulates myoblast function *in vitro*,[21] leading to our hypothesis that plasminogen is a viable candidate to enhance tissue resilience during CR. Moreover, plasminogen activator inhibitor 1 (PAI-1), the negative regulator of plasmin generation, decreases during CR in the mouse,[22] and its function is inversely correlated with metabolic health and longevity in humans.[23] The role of plasminogen as a regulator of CR-related biology has not been described and could elucidate a tissue crosstalk mechanism between liver and muscle.

Several plasminogen receptors have been identified.[24–30] In skeletal muscle, α-enolase has been proposed to bind plasminogen in primary myoblasts and regulate plasma activation and associated myoblast fusion and muscle regeneration.[21,31] However, there is no evidence to suggest that α-enolase can generate downstream cellular signaling. The most recently identified plasminogen receptor is a transmembrane protein with a C-terminal lysine exposed on the cell surface of macrophages[32] and platelets,[33] referred to as the plasminogen receptor KT (Plg-R_{KT}).[32,34] This receptor is capable of downstream signal transduction[35] and serves as a candidate direct mechanism for plasminogen signaling on the satellite cell. Currently, no plasminogen receptor has been identified that regulates satellite cell proliferation, function, or downstream signaling in the context of CR.

This study demonstrates that short-term CR enhances liver protein secretion of plasminogen, which binds directly to the muscle satellite cell to promote proliferation and subsequent muscle resilience during CR.

RESULTS

CR promotes plasminogen secretion and activation

To achieve tissue-specific protein labeling, we crossed the *MetRS*^{L274G} transgenic mouse[13,14] with Cre lines specific to liver, skeletal muscle, or adipose tissue, generating a *MetRS*$^{L274G(+/-)}$ 3 Cre$^{(+/-)}$ mouse. Each mouse line was given a short-term (3-month) CR diet, and in the final week, the methionine surrogate azido-nor-leucine (ANL) was administered. This allowed us to label and isolate all proteins secreted by their respective tissue under *ad libitum* (AL) or CR diets (Figures 1A and 1B). The short-term CR diet resulted in a gradual reduction in body weight over the 3 months (Figure S1), similar to what has been reported previously.[8] Qualitative analysis of secreted proteins in plasma showed that the liver contributed the greatest quantity of labeled proteins under the AL diet; this is not surprising since the liver is the primary producer of plasma proteins. With this technique,

compared with background levels of labeled protein in plasma, we did not observe any contribution over background from either skeletal muscle or adipose tissue (Figure 1B). In mice fed a CR diet, we observed a robust induction of proteins secreted from the liver, which was not evident in proteins secreted by muscle or adipose tissue (Figure 1B).

From these data, we focused on liver-derived plasma proteins during CR. To maximize labeling for proteomics, we bred the *MetRS*^{L274G} transgene to homozygosity, generating a *MetRS*$^{L274G(+/+)}$/albumin Cre$^{(+)}$ mouse. The homozygous *MetRS*^{L274G} line gave more abundant labeling (Figure S2A) and, importantly, maintained the transgene only under Cre activation (Figure S2B). Using this mouse line, we collected blood at 2, 6, and 10 weeks of CR to determine the temporal nature of hepatic protein expression. We observed a similar expression pattern in plasma at 2, 6, and 10 weeks of CR (Figure S2C). We then performed quantitative mass spectrometry on the liver-derived proteins containing the ANL label at 10 weeks of CR (Table S1); this demonstrated a pronounced role of coagulation-related proteins, as these comprised more than half of the top Gene Ontology (GO) terms (Figure 1C). Our top downregulated GO terms were related to inflammatory processes (Figure S2D). At the individual protein level, we were not surprised to observe an effect of CR to increase several proteins involved in hemostasis, including kininogen-1, Serpind1, Serpinf2, vitronectin, and plasminogen (Figure 1D).

The emergence of plasminogen's role during tissue regeneration and wound healing[16,18,20] and known regulation of skeletal muscle progenitor function[16,31] helped generate our hypothesis that plasminogen could be a factor mediating the muscle satellite cell expansion and improved resilience under CR. We validated the increased circulating plasminogen expression after 10 weeks of CR via ELISA (Figure 1E). Although plasminogen is primarily secreted from the liver, other tissues have been reported to express plasminogen, including muscle, kidney, and adipose tissue.[16,36] To determine whether extrahepatic tissues were increasing plasminogen mRNA expression after CR, we measured transcript levels in muscle, white adipose tissue, liver, and kidney (Figure S2E). Only the liver showed an increased expression of plasminogen, giving support to the theory that the liver is the source of the hypersecretion of plasminogen.

In addition to plasminogen, we observed a reduction in circulating PAI-1, the negative regulator of plasminogen activation (Figure 1F), along with increases in the plasminogen-processing proteins tissue plasminogen activator (tPA; Figure 1G) and urokinase plasminogen activator (uPA; Figure 1H). Moreover, we observed an increase in plasma plasmin activity (Figure 1I), which indicated a systemic upregulation of the plasmin(ogen) pathway with CR.

Suppression of plasminogen secretion prevents satellite cell expansion during CR

We next aimed to determine whether the induction of liver plasminogen secretion is necessary for the satellite cell expansion seen with CR. We administered an AAV8 carrying shRNA (short hairpin RNA) to *Plg* in young mice 2 weeks before the short-term CR diet to knock down hepatic gene expression and subsequent secretion of plasminogen (Figure 2A). In AL-fed mice, the AAV (adeno-associated virus) decreased hepatic plasminogen gene expression and plasma protein expression by roughly 50% and 40%, respectively (Figures

2B and 2C). The AAV-induced knockdown of plasminogen did not affect circulating PAI-1, uPA, or plasmin activity, as these levels were not different from the scrambled control group (Figures S3A–S3C). In CR mice, the knockdown returned both liver gene expression and secreted plasminogen protein back to AL levels (Figures 2B and 2C). Again, the knockdown did not affect CR-related reduction in PAI-1 or increase in uPA secretion (Figures S3A and S3B) but did reduce plasma plasmin activity (Figure S3C). We also measured *Plg* expression in muscle, kidney, and adipose tissue in all four groups to ensure specific targeting of the knockdown to the liver since plasminogen expression, although negligible, has been reported in these tissues.[36] We observed little effect of CR or the shRNA AAV on *Plg* mRNA expression across all tissues (Figures S3D and S3F).

Short-term CR has been shown to increase muscle satellite cell number and enhance early-stage muscle regeneration capacity.[8,10,11] We were able to repeat these findings, as 3 months of CR increased satellite cell numbers, as quantified by flow cytometry (Figures 2D–2F) and histology (Figures S3G and S3H). The knockdown of plasminogen had no effect on satellite cell numbers of AL-fed mice (Figures 2E and 2F) but prevented CR-induced satellite cell expansion (Figures 2D–2F, S3G, and S3H). To determine the regenerative consequences of plasminogen knockdown during CR, we injured the tibialis anterior (TA) muscle with $BaCl_2$ and quantified the cross-sectional area (CSA) of myofibers positive for the early regenerative marker embryonic myosin heavy chain (eMHC) 5 days after injury. In the scrambled control AAV groups, the TAs from CR-fed mice showed enhanced recovery with a 31% increase in CSA of eMHC(+) fibers compared with AL mice (Figures 2G and 2H). With the plasminogen knockdown, the CR effect was lost, and the TA CSA was similar to that of AL-fed mice (Figures 2G and 2H). Hypersecretion of plasminogen appears to be necessary for CR-induced satellite cell expansion and enhanced early myogenic recovery. To investigate the effect of plasminogen knockdown on a later time point of regeneration, we measured the myofiber CSA 30 days post injury (Figures 2I and 2J). To account for differences in pre-injury CSA between AL and CR TA muscle, we normalized the CSAs to their respective uninjured values and presented the data as a percentage change compared with the uninjured TA muscle. We observed an increase of 15% in CSA in the AL-fed scrambled control AAV group, which was partially attenuated following plasminogen knockdown. In contrast, the CR-fed scrambled control AAV group did not hypertrophy beyond uninjured values, while the plasminogen knockdown group showed a significant reduction in CSA, preventing the return to pre-injury values.

Plasminogen signals directly to the satellite cell, activating ERK

Next, we sought to determine whether plasminogen signals directly to satellite cells. Activation of the ERK (extracellular signal-regulated kinase) pathway has been reported after plasminogen treatment of fibroblasts.[37] Moreover, ERK signaling is involved in satellite cell proliferation,[38] leading us to focus on ERK as a potential downstream signaling node regulating the CR outcomes. For *in vitro* signaling experiments, satellite cells were isolated from both AL and CR-fed mice, plated in serum-free medium, and treated with recombinant plasminogen. Plasminogen treatment of AL satellite cells moderately induced ($p = 0.09$) phospho-ERK (p-ERK); however, treatment of CR satellite cells produced a synergistic 2-fold increase in p-ERK (Figure 3A). To associate ERK activation with

proliferative function, we aimed to determine the effect of plasminogen treatment on proliferation of cells isolated from AL and CR mice. Plasminogen treatment did not affect proliferation of cells from AL mice (Figure 3B). In contrast, CR increased proliferation of satellite cells independent of plasminogen treatment and showed a further 57% increase in proliferation with plasminogen treatment (Figure 3B). We next demonstrated that ERK signaling was necessary for the proliferative effects of CR and plasminogen treatment. Satellite cells from AL- and CR-fed mice were treated with or without the ERK inhibitor LY3214996 (Figure 3C). Inhibition of ERK reduced proliferation in AL satellite cells regardless of plasminogen treatment (Figure 3C). ERK inhibition had similar effects on CR satellite cells as the induction of proliferation with CR, and the further increase with plasminogen treatment was negated with ERK inhibition (Figure 3C). Since downstream ERK signaling appears to be necessary for plasminogen-induced satellite cell proliferation, we tested how these manipulations would affect typical gene markers of satellite cell/myoblast proliferation. Plasminogen treatment of satellite cells from AL-fed mice had no effect on the proliferation markers Myf5, CyclinD1, or MyoD (Figures 3D–3F). ERK inhibition reduced proliferation gene expression in AL satellite cells regardless of plasminogen treatment (Figures 3D–3F). Satellite cells from mice fed a CR diet showed a modest 58%, 82%, and 87% increase in Myf5, CyclinD1, and MyoD, respectively (Figures 3D–3F). With plasminogen treatment, we observed a more robust induction of gene markers of satellite cell proliferation, which was ablated with concurrent ERK inhibition (Figures 3D–3F).

The plasminogen receptor Plg-R_{KT} regulates downstream signaling and proliferation

Our next question was to identify the receptor through which plasminogen is signaling. CR induced several genes in satellite cells related to plasminogen activation, including the receptor uPAR and the plasminogen receptor Plg-R_{KT} (Figure 4A). This gene expression pattern was specific to satellite cells, as we did not see any effect of CR on whole-muscle gene expression (Figure S4A). In agreement with our gene expression data, we observed a low protein expression of Plg-R_{KT} in satellite cells sorted from AL-fed mice but a nearly 4-fold increase in Plg-R_{KT} protein in satellite cells sorted from mice on the CR diet (Figure 4B). We confirmed the increased protein abundance at the cell surface through histology and fluorescence-activated cell sorting (FACS) analysis. Using immunofluorescence on cultured satellite cells, we again observed a low expression of Plg-R_{KT} in satellite cells isolated from AL-fed mice (Figures S4B and S4C). After CR, we observed an increased protein expression of Plg-R_{KT} (Figures S4B and S4C). Supporting these data, our FACS analysis showed that CR resulted in a robust induction in the frequency and intensity of Plg-R_{KT} expression in freshly isolated satellite cells (Figure 4C). Interestingly, this effect was again specific to the satellite cell. We measured Plg-R_{KT} expression on other cell types in muscle, including fibro-adipogenic progenitors (FAPs), myeloid cells, and endothelial cells. We did not observe any differences in the expression of Plg-R_{KT} (Figures S4D and S4E) between cells isolated from mice fed AL and CR diets or the percentage of each cell type (Figure S4F).

After validation of both mRNA and protein expression of Plg-R_{KT} on the satellite cell, we aimed to determine downstream signaling after plasminogen treatment. To test whether the

ERK signaling is dependent on Plg-R_{KT}, we put both wild-type and Plg-R_{KT} knockout (KO) mice on short-term CR and treated their sorted satellite cells with recombinant plasminogen. We again observed a robust induction in p-ERK of the CR satellite cells; however, this effect was lost in the CR Plg-R_{KT} KO cells (Figure 4D). To determine whether Plg-R_{KT} was required for the proliferative effects of CR and/or plasminogen treatment, we added plasminogen to satellite cells sorted from AL- or CR-fed wild-type or Plg-R_{KT} KO mice. The loss of Plg-R_{KT} had no effect on satellite cell proliferation in AL-fed mice. However, the loss of Plg-R_{KT} prevented the proliferative effects of plasminogen on the CR cells (Figure 4E).

We next asked whether plasminogen is sufficient to signal to the satellite cell or whether active plasmin is needed. It appears that satellite cells from CR-fed mice have increased capacity to activate plasminogen, as plasmin activity is increased in the medium after plasminogen treatment (Figure S5A). This effect was not seen in the medium from satellite cells from mice on the AL diet. Furthermore, the loss of Plg-R_{KT} prevented the CR-induced increase in plasmin activity (Figure S5B). Based on these data, both plasminogen and plasmin are available in the medium to signal to CR satellite cells. To test each individual effect on ERK signaling, we treated satellite cells from CR-fed mice with either plasminogen or plasmin at similar doses. We observed similar effects of ERK activation with each signaling molecule (Figure 4F). Moreover, activation of ERK upon treatment with either plasminogen or plasmin was lost with the deletion of Plg-R_{KT} (Figure 4F). In regards to proliferation, we observed similar outcomes, as treatment with either plasminogen or plasmin increased proliferation to a similar extent, which was again lost in the Plg-R_{KT} KO cells (Figure 4G).

As our *in vitro* data demonstrated that plasminogen acted directly on satellite cells only after CR, we hypothesized the induction of Plg-R_{KT} is necessary for the CR effect on muscle satellite cell number and regeneration *in vivo*. Using the same CR regimen and time course as in the previous experiment, we put wild-type and Plg-R_{KT} KO mice on AL or CR diets for 3 months (Figure 5A). The loss of Plg-R_{KT} did not affect circulating plasminogen (Figure 5B), PAI-1 (Figure 5C), or uPA (Figure S5D) proteins under AL or CR diets. However, it did reduce plasma plasmin activity in both AL- and-CR fed mice (Figure S5E). Deletion of Plg-R_{KT} had no effect on satellite cell numbers in the AL-fed mice but prevented the CR-induced expansion of satellite cells when analyzed as a percentage of total cells or satellite cells per gram of tissue (Figures 5D–5F). Furthermore, the loss of Plg-R_{KT} perturbed the early regenerative process. AL-fed Plg-R_{KT} KO mice had a reduction in CSA of eMHC(+) fibers 5 days after $BaCl_2$ injury. The Plg-R_{KT} KO mice also failed to show any improvements of CSA with CR (Figures 5G and 5H).

Human CALERIE samples show increased circulating plasminogen and muscle stem cell expansion with CR

To validate whether plasminogen and/or related factors are altered in human plasma under a CR diet, we analyzed samples from the NIH CALERIE trial. CR participants were prescribed a 25% reduction in caloric intake from baseline, but actual CR achieved varied among participants. Thus, we stratified participants based on actual percent CR

and presented the data as percent change from their baseline value. For circulating measurements, we used three groups as follows: isocaloric (0% CR), moderate CR (7%–12% CR), and high CR (13%–35% CR). We measured plasma plasmin activity as a global measure of plasminogen processing. We observed an increase in plasmin activity in both moderate and high CR groups (Figure 6A), which was correlated with percent CR (Figure 6B). These data corresponded with an increase in circulating plasminogen in both moderate and high CR groups (Figure 6C), which was also correlated with the extent of CR (Figure 6D). In contrast, circulating PAI-1 levels, similar to what we observed in the mouse, were reduced in the high CR group (Figure 6E), which was negatively correlated with the percent CR (Figure 6F).

In support of the circulating PAI-1 data, we also conducted analysis of predicted PAI-1 protein secretion from blood and adipose DNA methylation datasets using a published algorithm (hereafter called DNAmPAI-1[39]). Since the methylation data were generated previously by Waziry et al.,[40] we maintained a 12-month completer analysis, keeping all subjects in their preassigned groups, who provided samples at baseline and the 12-month follow-up. In blood analyses, consistent with analyses of circulating PAI-1, CR was associated with downregulation of DNAmPAI-1 levels at the 12-month follow-up (Figure 6G). In adipose tissue analyses, there were no differences in DNAmPAI-1 at the 12-month follow-up (Figure 6H), which suggests that the changes we observed in circulating PAI-1 at 12 months of CR may not be due to CpG-site DNA methylation alterations in adipose tissue.

We next investigated whether the muscle phenotypes persisted in the CALERIE participants. For these experiments, we analyzed muscle biopsies from a subpopulation of the subjects who provided blood samples. We again assigned groups used for muscle histology measurements based on actual CR by the 12-month follow-up, which included isocaloric (0%CR) controls and high CR (19%–32% CR) participants. Compared with baseline values, CR was associated with a reduction in muscle cross-sectional fiber area (Figures 7A and 7B). There was no difference in fiber area between baseline and 12 months in the isocaloric group. Since CR increases muscle satellite cell numbers in rodent models, we investigated this phenomenon in humans. We observed a 30% increase in muscle satellite cell numbers after 12 months of CR compared with baseline; this was evident by the number of Pax7-positive cells normalized to fiber number (Figure 7C). We did not observe any increase in satellite cells in the isocaloric subjects (Figure 7C). In addition to satellite cell numbers, we measured the expression of Plg-R_{KT} on satellite cells to again determine whether our observations in the mouse would translate to human CR. Satellite cell Plg-R_{KT} expression in human muscle also increased by 69% after 12 months of CR, while there was no change in the isocaloric group (Figures 7D and 7E). To determine whether gene expression changes related to plasminogen activation would be detected in whole-muscle CALERIE samples, we use RNA sequencing (RNA-seq) data from Das et al.[41] Similar to the mouse data, whole-muscle mRNA expression of plasminogen receptor or genes related to plasminogen activation (PLAUR, PLAU, PLAT, or PLGRKT) was not altered by CR (Figure 7F). Taken together, the human CALERIE samples recapitulated several phenotypes of our murine data across blood and muscle tissues.

DISCUSSION

Using an unbiased proteomics approach, we report here that CR promotes a hypersecretion of proteins from the liver, including those involved in coagulation and fibrinolysis. We also demonstrated the role of liver-derived plasminogen in mediating satellite cell expansion and enhanced muscle regeneration during CR. We showed that the mediation was accomplished by an upregulation of the plasminogen receptor Plg-R_{KT} specifically on muscle satellite cells, promoting downstream ERK signaling and subsequent proliferation. We therefore propose that CR induces a distinct crosstalk between liver and muscle that increases muscle resilience.

The majority of studies examining the mechanism of CR action have focused on intrinsic cellular effects across different tissues.[2,42,43] Using the MetRS^{L274G}/bio-orthogonal non-canonical amino acid tagging (BONCAT) model to characterize an organ-specific secretome *in vivo*, our study aimed to investigate the systemic and extracellular effects of CR and how this could alter tissue resilience. We chose to investigate metabolic tissues with known effects of CR, including liver, skeletal muscle, and adipose tissue. We were intrigued by the induction of secreted proteins from the liver with CR, which was not evident in proteins secreted by either adipose or muscle tissues. The induction of the secretome was observed just 2 weeks after CR and continued throughout the 3-month CR period. Interestingly, CR increased secretion of proteins associated with the resolution of both coagulation and hemostasis. Although not the focus of this paper, these findings suggest increased secretion of fibrinolytic factors from the liver as a possible mechanism to improve cardiovascular health with CR, given that elevated hemostatic factor levels are typically associated with worsened clinical cardiovascular outcomes, such as increased risk of cardiovascular death.[44] Conversely, CR dampened secretion of proteins associated with increased inflammation, which is consistent with known anti-inflammatory effects of CR[45] and further validates our proteomics approach.

Our serum proteomics analysis identified several liver-derived secreted proteins increased with CR. Since we were searching for factors to promote satellite cell expansion and muscle regeneration, the supporting evidence for the plasminogen/plasmin system in wound repair and tissue resilience[16–20] led to our focus on plasminogen. It is also worth noting that plasmin has been shown to promote myoblast proliferation and fusion *in vitro*,[21] giving more support to the focus on plasminogen as a mediator of liver-muscle crosstalk during CR. Here, our knockdown experiments showed the necessity of plasminogen hypersecretion to expand the satellite cell pool during CR, even in the absence of acute injury.

In addition to the increased circulating plasminogen, we observed a reduction in circulating PAI-1 protein during CR. PAI-1 inhibits the activation of plasminogen by inhibiting both tPA and uPA. Time-restricted feeding promotes *plasminogen* gene expression in the mouse liver,[46] signifying that plasminogen could be secreted under conditions of metabolic stress. In contrast, PAI-1 levels have been shown to be inversely correlated with metabolic health and longevity in humans.[23] PAI-1 is also known to be a key contributor to the senescence-associated secretory phenotype (SASP) and has been shown to be both a marker and mediator of senescence.[47] In addition to increased plasminogen secretion, we observed

increased circulation of tPA and uPA and elevated levels of plasma plasmin activity as a result of CR. The broad level of activation of the plasminogen system during CR suggests targeting of multiple tissues, as we do not believe that the plasminogen activation on the satellite cell is sufficient to increase circulating plasmin activity. Further research is needed to understand which tissues are also processing plasminogen and which biological functions are affected as a result.

Our work indicates that CR sensitized satellite cells to plasminogen by the upregulation of the plasminogen receptor Plg-R_{KT} and related processing proteins. While several plasminogen receptors have been identified,[24–30,32,34] we focused on Plg-R_{KT}[32,34] since it is a validated transmembrane protein with a C-terminal lysine[32] with known signaling transduction.[34] Alpha-enolase has been suggested as a functional plasminogen receptor on myoblasts.[21,31] However, α-enolase appears to play a more prominent role in myoblast differentiation and not during proliferation,[21] which appears to be the relevant mechanism during CR. Moreover, α-enolase lacks a transmembrane domain and has no known signaling capacity. While the current study does not rule out a role of α-enolase in plasminogen activation under CR, we do not believe that it serves as a key signaling receptor for satellite cell activation. Interestingly, Plg-R_{KT} expression decreased in adipose tissue and adipocytes in mice on a high-fat diet,[48] suggesting an inverse association between caloric intake and plasminogen sensitivity in certain cell types. Taken together, these results show substantial changes in Plg-R_{KT} expression and related signaling in response to caloric challenges to promote proliferation in the satellite cell under CR.

Plasminogen treatment increased ERK signaling only in satellite cells isolated from CR mice with high Plg-R_{KT} expression. Downstream ERK signaling and satellite cell proliferation with plasminogen treatment were dependent on the presence of Plg-R_{KT}. Although ERK signaling increases after plasminogen treatment of fibroblast cell lines,[37] no downstream signaling pathway has been established in the satellite cell. Considering that the ERK signaling pathway regulates satellite cell proliferation and not fusion,[38] it is reasonable to suggest that ERK signaling is activated during CR, where we see proliferation and expansion in cell numbers. Furthermore, we demonstrated the importance of Plg-R_{KT} when the Plg-R_{KT} KO mouse failed to show expanded satellite cell numbers or enhanced regeneration after CR despite elevated circulating plasminogen.

To demonstrate the relevance of our findings to human biology, we analyzed tissues from the CALERIE trial of human CR. We observed replication of many of the mouse phenotypes, including increased circulating plasminogen, decreased PAI-1, satellite cell expansion, and increased Plg-R_{KT} expression on the satellite cells of human CALERIE study participants. PAI-1 is increased with obesity in humans and reduced with weight loss,[49] but here we show a reduction in circulating PAI-1 in healthy adults after CR. This study also reports the expansion of satellite cells in human muscle with CR. This finding is critical to suggest translational relevance to the rodent data observed for more than a decade. Moreover, the increased expression of the plasminogen receptor Plg-R_{KT} observed on human satellite cells during CR provided additional support for the theory that our rodent model is relevant to human biology.

In summary, the MetRS model is a powerful approach that has been used to interrogate cell/tissue-specific proteomes in *C. elegans*,[50] *Drosophila melanogaster*,[51] and *Mus musculus*.[14] We now demonstrated how this model can also be used to characterize organ-specific secretomes *in vivo*, an approach we plan to extend to other organ systems and interventions. We demonstrated that plasminogen plays a critical role in mediating the stimulatory effects of CR on satellite cell proliferation and skeletal muscle resilience through the Plg-R_{KT} receptor.

Limitations of the study

A limitation of this study is that we only evaluated the effects of one type of short-term CR. Recent work by Acosta-Rodríguez et al.[5] has demonstrated significant differential effects of different types of CR on gene expression profiles and longevity. Importantly, they demonstrated that mice fed at night experienced the greatest increase in longevity. Given that the mice in this study were all fed during the day, it would therefore be useful to repeat this study using CR mice fed at night and/or under different durations of CR.

A further limitation of this study is our approach to track organ-specific secretomes using the MetRS mouse. We understand the difficulties surrounding plasma proteomics and acknowledge that the technique will not identify all secreted proteins/peptides from each tissue. We used this technology to identify changes in plasma protein secretion patterns with CR and to investigate whether any secreted proteins were differentially secreted with CR. We do not claim or believe that our proteomics coverage is comprehensive of the liver secretome. Moreover, recent studies have utilized additional approaches to measure plasma proteins in a tissue-specific manner. Yang et al.[52] described the development of a transgenic mouse model that expresses an endoplasmic reticulum-directed biotin ligase, BirA*G3, that can be used to characterize the secretomes of individual organs, including the liver. In addition, Wei et al.[53] used a proximity biotinylation strategy to label proteins in a cell-type-selective method. A comparison of these techniques would be valuable to understand the relative merits and weaknesses of our model compared with this approach.

Finally, our study used only male mice, while our human cohort from CALERIE used both men and women. Gender differences in longevity and various outcomes of CR have been reported across species.[54–56] While our human data are reassuring, the conclusions from our mouse results may or may not be relevant to females on a CR diet. Further investigation is needed to determine whether similar effects across genders can be observed under a similar CR regimen.

STAR★METHODS

RESOURCE AVAILABILITY

Lead contact—Further information and requests for reagents/resources should be directed to and will be fulfilled by the lead contact, James White (james.white@duke.edu).

Materials availability—Unique reagents generated in this study will be made available under a standard material transfer agreement on request from the lead contact.

Data and code availability

- All proteomic data generated or analyzed during this study are included in this published article (and its supplemental information files) and have been uploaded to ProteomeXchange with identifier PXD043644. Human skeletal muscle RNA-seq data were deposited in CALERIE bio repository that they can be obtained by request from the CALERIE bio repository.
- This study did not generate original code.
- Any additional information required to reanalyze the data reported in this manuscript is available from the lead contact upon request.

EXPERIMENTAL MODEL AND STUDY PARTICIPANT DETAILS

Mouse models—All animal care followed the guidelines and was approved by the Institutional Animal Care and Use Committees (IACUCs) at Duke Medical Center. Male C57BL/6J (Wild-type, Wt) mice were used at 2 months of age. Plg-R_{KT} gene targeted mice were backcrossed ten generations into the C57BL/6J background.[57] The Plg-R_{KT} mice were bred at heterozygosity and littermate Plg-R_{KT}(+/+) and Plg-R_{KT}(−/−) mice were used for experimental cohorts. The Skeletal alpha actin-Cre (#025750), Adiponectin-Cre (#028020) and Albumin-Cre (#003574) mice were purchased from Jackson laboratories. Mice containing the CAG-floxed-Stop-eGFP-mMetRS^{L274G} (MetRS*) transgene were a kind gift from the Schuman lab (Erin Schuman, Max Planck Institute for Brain Research, Frankfurt Germany), and details for the generation of this transgenic can be found in.[14] We refer to these mice simply as “MetRS” in this manuscript. All Cre and MetRS mice were initially crossed to generate heterozygous mice that were used for preliminary experiments. F1 progeny containing both the Albumin-Cre and MetRS alleles were crossed to eventually generate mice that were homozygous for the MetRS allele. Male mice with homozygous MetRS alleles were used for subsequent experiments as indicated in the main text and elsewhere in the methods section. All genotyping was performed by Transnetyx (Tennessee, USA) using tail snips.

Muscle stem cell isolation—Mouse muscles (triceps, quadriceps, hamstrings, tibialis anterior, gastrocnemius, soleus and plantaris) were collected, digested and prepared into a single cell suspension for flow cytometry or fluorescence-activated cell sorting (FACS) using the methods detailed by Liu et al.[58] Muscles were dissected, minced using scissors, digested in 10mL of F10 + 10%(v/v) horse serum and 1000U/mL Collagenase, Type 2 (Worthington) for 60 min at 37C in a shaking water bath, washed in F10 media, digested again for 30 min at 37C in F10 + 10%(v/v) horse serum +1.1U/mL dispase (Gibco) and 100U/mL type 2 collagenase, washed, passed through 40uM cell strainer and stained with antibodies for flow cytometry. Cells were identified using flow cytometry by forward scatter and side scatter parameters. Muscle stem cells were identified as APC-(CD45, CD11b, CD31, TER119) negative, FITC-SCA1 negative, and PE-CD106(VCAM1) positive. Flow cytometry and FACS were performed on Sony MA900 cell sorter equipped with 4 lasers and appropriate detector filter sets. Cell sorting was performed in a biosafety cabinet at 4C using 100uM microfluidic chip at a pressure near 20PSI. Cells were collected in media used

for culturing but washed once prior to seeding to remove FACS sorting sheath fluid. All antibodies used for these experiments are listed in the Key Resources Table.

CALERIE subjects—The Comprehensive Assessment of the Long-term Effects of Reducing Intake of Energy (CALERIE) trial (clinical trial registry # NCT00427193) randomized 220 healthy, non-obese (BMI 22.0 % BMI <28.0 kg/m^2), adults aged 21–50 years to either a 25% caloric restriction (CR) intervention condition or *ad libitum* (AL) control at a 2:1 (CR:AL) ratio across three sites (Pennington Biomedical Research Center, Washington University, and Tufts University)(Rickman et al., 2011; Rochon et al., 2011). Participants were excluded from the study if they had significant medical conditions, abnormal laboratory markers, present or potential psychiatric or behavioral problems, regular use of medications (except oral contraceptives), currently smoked, were highly physically active, or were pregnant or breastfeeding. Randomization was stratified by study site, sex and BMI. The trial duration was 24 months.[59] Further information about the CALERIE trial can be found at https://calerie.duke.edu. Throughout this study, a subset of participants were used based on their tissue availability and/or percentage caloric restriction. More detail on the study design and N's can be found in the results and respective figure legends.

METHOD DETAILS

Mouse model of caloric restriction—Mice were raised on an *ad libitum* diet and switched to CR at 2 months of age. Mice were then subjected to 3 months of CR (1 week at 20% restriction followed by 10–11 week at 40% restriction as in [8].) All mice were fed daily between 8 and 9 a.m., and monitored weekly for any abnormal weight loss.

Flow cytometry and cell sorting—Mouse muscles (triceps, quadriceps, hamstrings, tibialis anterior, gastrocnemius, soleus and plantaris) were collected, digested and prepared into a single cell suspension for flow cytometry or fluorescence-activated cell sorting (FACS) using the methods detailed by Liu et al.[58] Muscles were dissected, minced using scissors, digested in 10mL of F10 + 10%(v/v) horse serum and 1000U/mL Collagenase, Type 2 (Worthington) for 60 min at 37C in a shaking water bath, washed in F10 media, digested again for 30 min at 37C in F10 + 10%(v/v) horse serum +1.1U/mL dispase (Gibco) and 100U/mL type 2 collagenase, washed, passed through 40uM cell strainer and stained with antibodies for flow cytometry. Cells were identified using flow cytometry by forward scatter and side scatter parameters. Muscle stem cells were identified as APC-(CD45, CD11b, CD31, TER119) negative, FITC-SCA1 negative, and PE-CD106(VCAM1) positive. Flow cytometry and FACS were performed on Sony MA900 cell sorter equipped with 4 lasers and appropriate detector filter sets. Cell sorting was performed in a biosafety cabinet at 4C using 100uM microfluidic chip at a pressure near 20PSI. Cells were collected in media used for culturing but washed once prior to seeding to remove FACS sorting sheath fluid. All antibodies used for these experiments are listed in the Key Resources Table.

Muscle injury—Barium chloride ($BaCl_2$) was used to induce muscle damage in tibialis anterior muscle (TA) via intramuscular injection of 30uL of 1.2%(v/v) $BaCl_2$ in PBS using

30g needle.[12] Uninjured controls were injected with an equal volume of PBS. The TA was allowed 5 or 30 days of recovery after injury for histological assessment.

Satellite cell culture—Satellite cells were isolated as described above and seeded in plates coated with collagen I (1 μg mL−1, BD Bioscience) and laminin (10 μg mL−1, BD Bioscience) in myogenic growth media (20% heat-inactivated horse serum, 1% pencillin/streptomycin and 5 ng mL−1 bFGF in F10). 384-well plates were used for all EdU proliferation assays using ~2,000 cells per well. 24-well plates were used for signaling experiments using ~150,000 cells. Cells were treated with recombinant plasminogen (Abcam) at 5 μg/ml or 54 nmol/L or plasmin (Abcam) at 5 μg/ml or 57 nmol/L. Additional groups were treated with the ERK inhibitor LY3214996 (MedChemExpress) at 2.3 μg/ml or 5 μmol/L.

Immunoblotting—Protein extraction and immunoblot were performed as previously described.[60] Proteins were resolved on SDS-PAGE and transferred to nitrocellulose membranes (Thermo Fisher Scientific). All primary antibodies were added at a concentration of 1:1000. Proteins were visualized on an Odyssey western blot imager (LI-COR) or chemiluminescence film. All antibodies and materials used for immunoblotting in this manuscript can be found in the STAR Methods section.

Real time qPCR—RNA extraction was performed using TRIzol reagent following manufacturer's instructions (Thermo Fisher Scientific). Reverse transcription was performed using the High-Capacity cRNA Reverse Transcription Kit following manufacturer's instructions (Thermo Fisher Scientific). Real-time PCR was performed on Quant Studio 6 system (Life Technologies) using Power SYBR Green PCR mastermix (Life Technologies) All primers used in this manuscript can be found in Table S2.

Histology and IF in muscle cryosection—OCT-mounted muscle sections (10 μm) were cut on a cryostat and dried at room temperature for 10 min. Sections were then blocked for 0.5 h with 10% goat serum, followed by an overnight incubation with a mouse anti-eMHC antibody (Developmental Studies Hybridoma Bank (DSHB), AB_10571455, 1:50). After staining, slides were washed with TBS followed by a 1 h incubation with a goat anti-mouse Alexa Fluor 647 (Invitrogen, AB_2633282 1:1000). After staining, slides were washed with TBS and mounted with mounting medium containing DAPI (Vector Laboratories, cat. no. H-1200). Images were taken using a fluorescent microscope (Olympus IX70). For quantification, 3–4 images (20X) were taken per muscle, ~200 fibers and eMHC (+) myofibers were analyzed for CSA, 5 days after injury. For uninjured myofiber CSA, Pax7 and Plg-R_{KT} staining, OCT-mounted muscle sections (10 μm) were stained with Pax7 5ug/mml, (University of Iowa Developmental Studies Hybridoma Bank) and Plg-R_{KT} 1:100 (Invitrogen, Cat #: PA5-98932) overnight, followed by a 2-h incubation with anti mouse and rabbit secondary antibodies, respectively. Sample were washed by TBS and incubated with wheat germ agglutinin (WGA) Alexa Fluor 555 (1:1000) for 20 min, washed with TBS and mounted with mounting medium containing DAPI. Images were taken using a fluorescent microscope (Olympus IX70). For quantification of Pax7(+) satellites cells, Pax7(+)/DAPI(+) cells were counted in 3–4 images (20x, ~150 fibers) and normalized to the total fibers

per field. Plg-R_{KT} expression was measured by mean fluorescent intensity (MFI) of each Pax7(+)/DAPI(+) cell, normalized to the satellite cell CSA.

Myofiber cross-sectional area analysis—Myofiber cross-sectional analysis was performed as previously described.[61,62] In brief, digital images from WGA or eMHC stained muscle sections (10 μm) a 20X magnification were taken and analyzed for fiber cross-sectional area using cellSens Dimension Desktop 1.7 (Olympus). Each fiber was traced with a handheld mouse and the number of pixels traced was calibrated to a defined area in micrometers squared. The researcher, blinded to the group, traced approximately 150 fibers per sample. All fibers in the cross-sectional images were quantified unless the sarcolemma was not intact.

EdU labeling—For EDU incorporation assay, EdU was added to culture media at 10uM at indicated time. Cells were incubated with EdU for ~12 h before fixation with 10% formalin. Click reaction was used to conjugate EdU with AZDye488 using Click Chemistry 488 imaging Kit per manufacturer instructions (Cat# 1350, Click Chemistry Tools, Scottsdale, AZ, USA) and imaged using FITC and DAPI fluorescence filter sets on Olympus Epifluorescent, inverted microscope.

***In vivo* ANL administration—**Deep labeling of *in vivo* proteomes was achieved by administering ANL (Jena Bioscience #CLK-AA009-500) at a concentration of 0.2 mmol/kg via daily IP injections for 6 days via IP injection. Tail vein blood draws were performed one day after the final injection using Sarstedt Microvette CB300 LH capillary blood collection tubes (Fisher Scientific# NC9046728). Plasma was collected from the tubes following manufacturer's instructions, and either immediately used or frozen.

Bio-orthogonal non-canonical amino acid tagging (BONCAT)—Plasma proteins were biotinylated as described in [15] using the Click-&-Go Protein Reaction Buffer Kit following manufacturer's instructions (Click Chemistry Tools #1262). Biotinylated proteins were visualized via western blotting using IRDye 800CW Streptavidin at a concentration of 1:1000 (LI-COR). For detection and quantification via mass spectrometry, biotinylated proteins were enriched by affinity purification using Dynabeads MyOne Streptavidin C1 (ThermoFisher #65001) as described in [63].

MS sample preparation and analyses

Sample preparation: Samples were supplemented with SDS for a final concentration of 5% for digestions and spiked with undigested casein at a total of 120 or 240 fmol. Samples were then reduced with 10 mM dithiothreitol for 30 min at 80C and alkylated with 20 mM iodoacetamide for 30 min at room temperature. Next, they were supplemented with a final concentration of 1.2% phosphoric acid and 517 μL of S-Trap (Protifi) binding buffer (90% MeOH/100 mM TEAB). Proteins were trapped on the S-Trap, digested using 20 ng/μL sequencing grade trypsin (Promega) for 1 h at 47C, and eluted using 50 mM TEAB, followed by 0.2% FA, and lastly using 50% ACN/0.2% FA. All samples were then lyophilized to dryness and resuspended in 12 μL 1% TFA/2% acetonitrile containing 12.5

fmol/μL yeast alcohol dehydrogenase. A QC Pool was created by taking 3 μL from each sample, which was run periodically throughout the acquisition period.

Quantitative analysis, methods: Quantitative LC/MS/MS was performed on 4 μL (25%) of each sample, using a nanoAcquity UPLC system (Waters Corp) coupled to a Thermo Orbitrap Fusion Lumos high resolution accurate mass tandem spectrometer (Thermo) via a nanoelectrospray ionization source. Briefly, the sample was first trapped on a Symmetry C18 20 mm × 180 μm trapping column (5 mul/min at 99.9/0.1 v/v water/acetonitrile), after which the analytical separation was performed using a 1.8 μm Acquity HSS T3 C18 75 μm × 250 mm column (Waters Corp) with a 90-min linear gradient of 5–30% acetonitrile with 0.1% formic acid at a flow rate of 400 nL/min (nL/min) with a column temperature of 55C. Data collection on the Fusion Lumos mass spectrometer was performed in a data-dependent acquisition (DDA) mode of acquisition with an r = 120,000 (@ m/z 200) full MS scan from m/z 375–1500 with a target AGC value of 4e5 ions. MS/MS scans were acquired at Rapid scan rate (Ion Trap) with an AGC target of 1e4 ions and a max injection time of 100 ms. The total cycle time for MS and MS/MS scans was 2 s. A 20s dynamic exclusion was employed to increase depth of coverage. The total analysis cycle time for each sample injection was approximately 2 h.

Quantitative LC-MS/MS analysis: Following UPLC-MS/MS analyses, data were imported into Proteome Discoverer 2.4 (Thermo Scientific Inc.) and analyses were aligned based on the accurate mass and retention time of detected ions (“features”) using Minora Feature Detector algorithm in Proteome Discoverer. Relative peptide abundance was calculated based on area-under-the-curve (AUC) of the selected ion chromatograms of the aligned features across all runs. The MS/MS data were searched against the SwissProt *M. musculus* database (downloaded in Nov 2019), and an equal number of reversed-sequence “decoys” for false discovery rate determination. Mascot Distiller and Mascot Server (v 2.5, Matrix Sciences) were utilized to produce fragment ion spectra and to perform the database searches. Database search parameters included fixed modification on Cys (carbamidomethyl) and variable modification on Meth (oxidation) and Asn and Gln (deamidation). Peptide Validator and Protein FDR Validator nodes in Proteome Discoverer were used to annotate the data at a maximum 1% protein FDR. Missing values were imputed after sample loading and trimmed-mean normalization in the following manner – if less than half of the values are missing in a treatment group, values are imputed with an intensity derived from a normal distribution defined by measured values within the same intensity range (20 bins). If greater than half the values are missing for a peptide in a group and a peptide intensity in > 5e6, then it was concluded that the peptide was misaligned and its measured intensity was set to 0. All remaining missing values are imputed with the lowest 5% of all detected values.

***In vivo* AAV8-mediated Plg knockdown—**The AAV8-U6-PLG-shRNA and scramble control vector were generated by Vector Biosystems (Malvern, PA). The AAV8 was administered via the tail vein at $1x10^{11}$ vector genomes per mouse, which was diluted in 100μls PBS.

Plasmin activity assay—Plasmin activity assays were performed on plasma (100 μg total protein) in 96-well black micro-assay plates (Greiner Lot: 08 27 01 15) using the Plasmin Activity Assay Kit (Fluorometric) following manufacturer's instructions (abcam #ab204728).

Mouse ELISA—Mouse plasminogen, PAI-1, tPA and uPA were measured by ELISA (Abcam: #ab198511, #ab197752, #ab233615 and #ab245727, respectively). Intra-assay CVs were ≤%7%.

CALERIE analysis

Human ELISA: Human plasminogen and PAI-1 proteins were measured by ELISA (Abcam: ab108893 and ab269373, respectively) as per manufacturer's instructions. Inter-assay CVs were <6% and intra-assay CVs were <3%.

DNA methylation analysis

Blood DNAm: DNA methylation (DNAm) profiling was conducted in the Kobor Lab from whole-blood DNA stored at −80°C. After quality controls and normalization, DNAm datasets were generated for n = 595 samples from 214 individuals (125 CR, 65 AL). Briefly, 750 ng of DNA was extracted from whole blood and bisulfite converted using the EZ DNA Methylation kit (Zymo Research, Irvine, CA, USA). Methylation was measured from 160 ng of bisulfite converted DNA using the Illumina EPIC Beadchip (Illumina Inc, San Diego, CA, USA). Quality control and normalization were performed using methylumi (v. 2.32.0) from the R statistical programming environment (v 3.6.3). Probes with detection p values >0.05 were coded as missing; probes missing in >5% of samples were removed from the dataset (final probe n = 828,613 CpGs). Normalization to eliminate systematic dye bias in the 2-channel probes was carried out using the methylumi default method).

Adipose DNAm—Adipose tissue was sampled according to protocols established by the CALERIE trial investigators (CALERIE Biorepository, 2007). Adipose tissue samples were obtained from the CALERIE biorepository and DNA was extracted using the Qiagen kit. DNAm profiling was conducted in the UNGC core facility at UCLA from adipose DNA stored at −80°C. After quality controls and normalization, DNAm datasets were generated for n = 86 samples from 43 individuals (29 CR, 14 AL). Briefly, 250 ng of DNA was extracted from adipose tissue samples and bisulfite converted using [the EZ DNA Methylation kit (Zymo Research, Irvine, CA, USA)]. Methylation was measured from 160 ng of bisulfite converted DNA using the Illumina EPIC Beadchip (Illumina Inc, San Diego, CA, USA). Normalization was performed using the normal-exponential out-of-band (noob) normalization method from the minfi package within the R statistical programming environment.[64]

DNAmPAI1—DNAmPAI1 is an algorithm-based measurement that predicts levels of PAI-1 in a tissue from DNA methylation data. DNAmPAI1 can be interpreted as an estimate of the quantity of PAI1 protein in the tissue. DNAmPAI1 was measured from blood and adipose DNAm datasets based on the algorithm developed from analysis of serum PAI1 in the Framingham Heart Study Offspring Cohort.[39] Blood and adipose DNAmPAI1 levels were

calculated using the Horvath Lab's online calculator (http://labs.genetics.ucla.edu/horvath/dnamage/).

DNAm estimates of immune cell composition of blood DNA samples— Estimates of immune cell counts (CD4T, CD8T, Natural Killer (NK), and B-cell lymphocytes, monocytes, and neutrophils) were computed from blood DNAm datasets using algorithms developed for the EPIC array by Salas et al.[65]

Muscle biopsies—Vastus lateralis biopsy samples (~150 mg) were taken after local anesthesia using the Bergstrom technique as previously described.[66] Fat and connective tissue were removed from the biopsy sample and muscle was snap frozen in liquid nitrogen and stored at −80°C.

RNA extraction—RNA extraction and sequencing were performed as previously described.[41] In brief, sections of frozen skeletal muscle (quadriceps) (~50 mg) were homogenized using bead-based Qiagen TissueLyser II in l mL TRIzol Reagent (Invitrogen ThermoFisher #15596026). Following homogenization, total RNA was extracted using Qiagen RNeasy Mini Kit (Qiagen #74104) and stored at −80°C.

Sample preparation and next generation sequencing—cDNA libraries were prepared from the extracted RNA and total RNA was isolated using QIAcube, Qiagen. Next, cDNA was synthesized using the NuGen Ovation v2 system. Illumina libraries were generated from the cDNA with the TruSeq Stranded Total RNA Library Preparation Kit and RNA was sequenced using Illumina NovaSeq 6000 sequencing system at a depth of >80 million paired-end reads. Sequencing data, in the form of FASTQ files, were filtered and aligned using BBDuk (decontamination using kmers), a program included in the BBTools suite (https://jgi.doe.gov/data-and-tools/software-tools/bbtools/). Short reads were aligned using STAR Aligner (version 2.7.10a) and then processed using featureCounts[67] from the Rsubread package (version 2.0.1).[68] Sequencing reads were then mapped to the reference human genome 38 (hg38) with Ensembl v104. The aligned reads were then filtered and normalized using the BioConductor package edgeR.[69] Briefly, raw sequencing counts (n = 19,900) were read into R (version 4.2.0; R Core team, 2020) and subsequently filtered to remove low expressors (n = 3,450) using a counts per million (CPM) threshold, corresponding to a row sum of ~50 counts while also requiring ≥2 samples to meet this threshold criteria to be included in the filtered dataset (n = 16,450). Following filtering, normalization factors were calculated using the trimmed mean of M-values (TMM) method, and dispersion was estimated.

QUANTIFICATION AND STATISTICAL ANALYSIS

Statistical analysis—Data were analyzed by two-tailed, unpaired Student's t-test for two-group comparisons, one-way ANOVA for three-group comparisons and two-way ANOVA for 4-group comparisons. Post hoc ANOVA analysis was performed using Tukey's post hoc analysis or targeted Student's t-test. Chi square analysis was performed to determine significant changes in myofiber cross sectional area. Linear regression analysis was performed to determine correlation coefficients and significance. All data are reported as

mean ± SEM or mean ± SDM. Statistical analysis was performed using GraphPad Prism 6 software. Exploratory data analysis and plotting was performed in R (version 4.0.5) and RStudio (version 1.4.1106). Statistical parameters, including number of biological replicates and statistical tests are reported in the figure legends.

Statistical analysis for DNAm—We tested CALERIE treatment effects on DNAmPAI1 following the method established by the CALERIE investigators.[70] Briefly, at the 12-month follow-up, we computed change scores by subtracting a participant's baseline from their DNAmPAI1 value at that assessment. Analysis included participants with data at baseline and at least one follow-up assessment (Blood n = 197; Adipose n = 48). We then fit linear mixed effects models to the change scores using the R package *lme4*.[71] Models included an indicator variable coding treatment group, an indicator variable coding the 12-month follow-up, and a product term for the interaction between treatment group and follow-up. Models included as covariates participants' ages at baseline, sex, BMI stratum (<25, 25–29), the first three principal components estimated from genome-wide SNP data, and participants' baseline levels of DNAmPAI1. For blood, an additional model specification was run that included DNAm estimates of immune cell counts (CD4T, CD8T, NK, Bcell, monocytes, and neutrophils). All models included a random intercept for subject ID. In this model, the coefficient for treatment group tests the effect of CALERIE intervention on DNAmPAI1 at 12-month. Treatment effect estimates were scaled according to the standard deviation of DNAmPAI1 at pre-treatment baseline to approximate a standardized treatment effect on the scale of Cohen's *D*.

Supplementary Material

Refer to Web version on PubMed Central for supplementary material.

ACKNOWLEDGMENTS

We thank all members of the White lab for valued discussions and insights on this project. J.L.H., manager of the Duke Pepper Center Biomarker Core, provided analyses for this project and was supported by NIH P30 AG028716. D.E.L. was supported by a training grant from the NIH (T32HL007057). J.P.W. was supported by NIH grants K01AG056664 and R21AG065943 and the Joe W. and Dorothy Dorsett Brown Foundation. L.A.M. was supported by NIH grant HL081046. L.A.M. and R.J.P. were supported by NIH grant HL149511. R.J.P. was supported by Merit Review Award I01BX003933 from the US Department of Veterans Affairs. W.E.K. and J.P.W. were supported by NIH grant P30 AG028716. K.M.H. and W.E.K. were supported by NIH grant R33 AG070455. D.W.B., J.P.W., K.M.H., and W.E.K. are supported by NIH grant R01AG061378. V.B.K. was supported by NIH P30 AG028716. The graphical abstract was generated with BioRender.

REFERENCES

1. Bareja A, Lee DE, and White JP (2019). Maximizing Longevity and Healthspan: Multiple Approaches All Converging on Autophagy. Front. Cell Dev. Biol 7, 183. [PubMed: 31555646]
2. Bareja A, Draper JA, Katz LH, Lee DE, Grimsrud PA, and White JP (2021). Chronic caloric restriction maintains a youthful phosphoproteome in aged skeletal muscle. Mech. Ageing Dev 195, 111443. [PubMed: 33529682]
3. Ham DJ, Börsch A, Chojnowska K, Lin S, Leuchtmann AB, Ham AS, Thürkauf M, Delezie J, Furrer R, Burri D, et al. (2022). Distinct and additive effects of calorie restriction and rapamycin in aging skeletal muscle. Nat. Commun 13, 2025. [PubMed: 35440545]
4. de Oliveira TQ, de Moura AC, Feistauer V, Damiani R, Braga MF, Almeida S, Guedes RP, and Giovenardi M (2022). Caloric restriction in mice improves short-term recognition memory and

modifies the neuroinflammatory response in the hippocampus of male adult offspring. Behav. Brain Res 425, 113838. [PubMed: 35283195]

5. Acosta-Rodríguez V, Rijo-Ferreira F, Izumo M, Xu P, Wight-Carter M, Green CB, and Takahashi JS (2022). Circadian alignment of early onset caloric restriction promotes longevity in male C57BL/6J mice. Science 376, 1192–1202. [PubMed: 35511946]
6. Al-Ajmi N, Saretzki G, Miles C, and Spyridopoulos I (2014). Dietary restriction ameliorates haematopoietic ageing independent of telomerase, whilst lack of telomerase and short telomeres exacerbates the ageing phenotype. Exp. Gerontol 58, 113–119. [PubMed: 25038516]
7. Li SJ, Lin YH, Chiang CH, Wang PY, and Chen CY (2022). Early-onset dietary restriction maintains mitochondrial health, autophagy and ER function in the left ventricle during aging. J. Nutr. Biochem 101, 108944. [PubMed: 35017002]
8. Cerletti M, Jang YC, Finley LWS, Haigis MC, and Wagers AJ (2012). Short-term calorie restriction enhances skeletal muscle stem cell function. Cell Stem Cell 10, 515–519. [PubMed: 22560075]
9. David CEB, Lucas AMB, Cunha PLO, Viana YIP, Yoshinaga MY, Miyamoto S, Filho ABC, Varela ALN, Kowaltowski AJ, and Facundo HT (2022). Calorie restriction changes lipidomic profiles and maintains mitochondrial function and redox balance during isoproterenol-induced cardiac hypertrophy. J. Physiol. Biochem 78, 283–294. [PubMed: 35023023]
10. Boldrin L, Ross JA, Whitmore C, Doreste B, Beaver C, Eddaoudi A, Pearce DJ, and Morgan JE (2017). The effect of calorie restriction on mouse skeletal muscle is sex, strain and time-dependent. Sci. Rep 7, 5160. [PubMed: 28698572]
11. Abreu P, Serna JDC, Munhoz AC, and Kowaltowski AJ (2020). Calorie restriction changes muscle satellite cell proliferation in a manner independent of metabolic modulation. Mech. Ageing Dev 192, 111362. [PubMed: 33010305]
12. White JP, Billin AN, Campbell ME, Russell AJ, Huffman KM, and Kraus WE (2018). The AMPK/p27(Kip1) Axis Regulates Autophagy/Apoptosis Decisions in Aged Skeletal Muscle Stem Cells. Stem Cell Rep 11, 425–439.
13. Liu Y, Conboy MJ, Mehdipour M, Liu Y, Tran TP, Blotnick A, Rajan P, Santos TC, and Conboy IM (2017). Application of bio-orthogonal proteome labeling to cell transplantation and heterochronic parabiosis. Nat. Commun 8, 643. [PubMed: 28935952]
14. Alvarez-Castelao B, Schanzenbächer CT, Hanus C, Glock C, Tom Dieck S, Dörrbaum AR, Bartnik I, Nassim-Assir B, Ciirdaeva E, Mueller A, et al. (2017). Cell-type-specific metabolic labeling of nascent proteomes in vivo. Nat. Biotechnol 35, 1196–1201. [PubMed: 29106408]
15. Alvarez-Castelao B, Schanzenbächer CT, Langer JD, and Schuman EM (2019). Cell-type-specific metabolic labeling, detection and identification of nascent proteomes in vivo. Nat. Protoc 14, 556–575. [PubMed: 30610240]
16. Suelves M, López-Alemany R, Lluís F, Aniorte G, Serrano E, Parra M, Carmeliet P, and Muñoz-Cánoves P (2002). Plasmin activity is required for myogenesis in vitro and skeletal muscle regeneration in vivo. Blood 99, 2835–2844. [PubMed: 11929773]
17. Bezerra JA, Bugge TH, Melin-Aldana H, Sabla G, Kombrinck KW, Witte DP, and Degen JL (1999). Plasminogen deficiency leads to impaired remodeling after a toxic injury to the liver. Proc. Natl. Acad. Sci. USA 96, 15143–15148. [PubMed: 10611352]
18. Drixler TA, Vogten JM, Gebbink MFBG, Carmeliet P, Voest EE, and Borel Rinkes IHM (2003). Plasminogen mediates liver regeneration and angiogenesis after experimental partial hepatectomy. Br. J. Surg 90, 1384–1390. [PubMed: 14598419]
19. Ny L, Parmer RJ, Shen Y, Holmberg S, Baik N, Bäckman A, Broden J, Wilczynska M, Ny T, and Miles LA (2020). The plasminogen receptor, Plg-RKT, plays a role in inflammation and fibrinolysis during cutaneous wound healing in mice. Cell Death Dis 11, 1054. [PubMed: 33311441]
20. Sulniute R, Shen Y, Guo YZ, Fallah M, Ahlskog N, Ny L, Rakhimova O, Broden J, Boija H, Moghaddam A, et al. (2016). Plasminogen is a critical regulator of cutaneous wound healing. Thromb. Haemost 115, 1001–1009. [PubMed: 26791370]
21. Díaz-Ramos À, Roig-Borrellas A, García-Melero A, Llorens A, and López-Alemany R (2012). Requirement of plasminogen binding to its cell-surface receptor alpha-enolase for efficient regeneration of normal and dystrophic skeletal muscle. PLoS One 7, e50477. [PubMed: 23239981]

22. Lijnen HR, Van Hul M, and Hemmeryckx B (2012). Caloric restriction improves coagulation and inflammation profile in obese mice. Thromb. Res 129, 74–79. [PubMed: 21689844]
23. Khan SS, Shah SJ, Klyachko E, Baldridge AS, Eren M, Place AT, Aviv A, Puterman E, Lloyd-Jones DM, Heiman M, et al. (2017). A null mutation in SERPINE1 protects against biological aging in humans. Sci. Adv 3, eaao1617. [PubMed: 29152572]
24. Miles LA, Dahlberg CM, Plescia J, Felez J, Kato K, and Plow EF (1991). Role of cell-surface lysines in plasminogen binding to cells: identification of alpha-enolase as a candidate plasminogen receptor. Biochemistry 30, 1682–1691. [PubMed: 1847072]
25. Hembrough TA, Vasudevan J, Allietta MM, Glass WF 2nd, and Gonias SL (1995). A cytokeratin 8-like protein with plasminogen-binding activity is present on the external surfaces of hepatocytes, HepG2 cells and breast carcinoma cell lines. J. Cell Sci 108, 1071–1082. [PubMed: 7542667]
26. Kassam G, Le BH, Choi KS, Kang HM, Fitzpatrick SL, Louie P, and Waisman DM (1998). The p11 subunit of the annexin II tetramer plays a key role in the stimulation of t-PA-dependent plasminogen activation. Biochemistry 37, 16958–16966. [PubMed: 9836589]
27. Herren T, Burke TA, Das R, and Plow EF (2006). Identification of histone H2B as a regulated plasminogen receptor. Biochemistry 45, 9463–9474. [PubMed: 16878981]
28. Hawley SB, Tamura T, and Miles LA (2001). Purification, cloning, and characterization of a profibrinolytic plasminogen-binding protein, TIP49a. J. Biol. Chem 276, 179–186. [PubMed: 11027681]
29. Dudani AK, and Ganz PR (1996). Endothelial cell surface actin serves as a binding site for plasminogen, tissue plasminogen activator and lipoprotein(a). Br. J. Haematol 95, 168–178. [PubMed: 8857956]
30. Miles LA, and Parmer RJ (2013). Plasminogen receptors: the first quarter century. Semin. Thromb. Hemost 39, 329–337. [PubMed: 23532575]
31. López-Alemany R, Suelves M, and Muñoz-Cánoves P (2003). Plasmin generation dependent on alpha-enolase-type plasminogen receptor is required for myogenesis. Thromb. Haemost 90, 724–733. [PubMed: 14515195]
32. Andronicos NM, Chen EI, Baik N, Bai H, Parmer CM, Kiosses WB, Kamps MP, Yates JR 3rd, Parmer RJ, and Miles LA (2010). Proteomics-based discovery of a novel, structurally unique, and developmentally regulated plasminogen receptor, Plg-RKT, a major regulator of cell surface plasminogen activation. Blood 115, 1319–1330. [PubMed: 19897580]
33. Whyte CS, Morrow GB, Baik N, Booth NA, Jalal MM, Parmer RJ, Miles LA, and Mutch NJ (2021). Exposure of plasminogen and a novel plasminogen receptor, Plg-RKT, on activated human and murine platelets. Blood 137, 248–257. [PubMed: 32842150]
34. Bai H, Baik N, Kiosses WB, Krajewski S, Miles LA, and Parmer RJ (2011). The novel plasminogen receptor, plasminogen receptor(KT) (Plg-R(KT)), regulates catecholamine release. J. Biol. Chem 286, 33125–33133. [PubMed: 21795689]
35. Vago JP, Sugimoto MA, Lima KM, Negreiros-Lima GL, Baik N, Teixeira MM, Perretti M, Parmer RJ, Miles LA, and Sousa LP (2019). Plasminogen and the Plasminogen Receptor, Plg-RKT, Regulate Macrophage Phenotypic, and Functional Changes. Front. Immunol 10, 1458. [PubMed: 31316511]
36. Zhang L, Seiffert D, Fowler BJ, Jenkins GR, Thinnes TC, Loskutoff DJ, Parmer RJ, and Miles LA (2002). Plasminogen has a broad extrahepatic distribution. Thromb. Haemost 87, 493–501. [PubMed: 11916082]
37. De Sousa LP, Brasil BSAF, Silva BM, Freitas MHA, Nogueira SV, Ferreira PCP, Kroon EG, and Bonjardim CA (2005). Plasminogen/plasmin regulates c-fos and egr-1 expression via the MEK/ERK pathway. Biochem. Biophys. Res. Commun 329, 237–245. [PubMed: 15721299]
38. Jones NC, Fedorov YV, Rosenthal RS, and Olwin BB (2001). ERK1/2 is required for myoblast proliferation but is dispensable for muscle gene expression and cell fusion. J. Cell. Physiol 186, 104–115. [PubMed: 11147804]
39. Lu AT, Quach A, Wilson JG, Reiner AP, Aviv A, Raj K, Hou L, Baccarelli AA, Li Y, Stewart JD, et al. (2019). DNA methylation GrimAge strongly predicts lifespan and healthspan. Aging (Albany NY) 11, 303–327. [PubMed: 30669119]

40. Waziry R, Ryan CP, Corcoran DL, Huffman KM, Kobor MS, Kothari M, Graf GH, Kraus VB, Kraus WE, Lin DTS, et al. (2023). Effect of long-term caloric restriction on DNA methylation measures of biological aging in healthy adults from the CALERIE trial. Nat. Aging 3, 248–257. [PubMed: 37118425]
41. Das J, Banskota N, Candia J, Griswold ME, Orenduff M, deCabo R, Corcoran DL, Das SK, De S, Huffman KM, et al. (2023). Calorie restriction modulates the transcription of genes related to stress-response and longevity in human muscle: the CALERIE study. Aging Cell
42. Miller BF, Robinson MM, Bruss MD, Hellerstein M, and Hamilton KL (2012). A comprehensive assessment of mitochondrial protein synthesis and cellular proliferation with age and caloric restriction. Aging Cell 11, 150–161. [PubMed: 22081942]
43. Morselli E, Maiuri MC, Markaki M, Megalou E, Pasparaki A, Palikaras K, Criollo A, Galluzzi L, Malik SA, Vitale I, et al. (2010). Caloric restriction and resveratrol promote longevity through the Sirtuin-1-depen-dent induction of autophagy. Cell Death Dis 1, e10. [PubMed: 21364612]
44. Morange PE, Bickel C, Nicaud V, Schnabel R, Rupprecht HJ, Peetz D, Lackner KJ, Cambien F, Blankenberg S, and Tiret L; AtheroGene Investigators (2006). Haemostatic factors and the risk of cardiovascular death in patients with coronary artery disease: the AtheroGene study. Arterioscler. Thromb. Vasc. Biol 26, 2793–2799. [PubMed: 17023678]
45. Gabande-Rodriguez E, Gómez de las M, Heras M, and Mittelbrunn M (2019). Control of Inflammation by Calorie Restriction Mimetics: On the Crossroad of Autophagy and Mitochondria. Cells 9.
46. Chaix A, Lin T, Le HD, Chang MW, and Panda S (2019). Time-Restricted Feeding Prevents Obesity and Metabolic Syndrome in Mice Lacking a Circadian Clock. Cell Metab 29, 303–319.e4. [PubMed: 30174302]
47. Vaughan DE, Rai R, Khan SS, Eren M, and Ghosh AK (2017). Plasminogen Activator Inhibitor-1 Is a Marker and a Mediator of Senescence. Arterioscler. Thromb. Vasc. Biol 37, 1446–1452. [PubMed: 28572158]
48. Samad F, Bai H, Baik N, Haider P, Zhang Y, Rega-Kaun G, Kaun C, Prager M, Wojta J, Bui Q, et al. (2022). The plasminogen receptor Plg-RKT regulates adipose function and metabolic homeostasis. J. Thromb. Haemost 20, 742–754. [PubMed: 34897983]
49. Folsom AR, Qamhieh HT, Wing RR, Jeffery RW, Stinson VL, Kuller LH, and Wu KK (1993). Impact of weight loss on plasminogen activator inhibitor (PAI-1), factor VII, and other hemostatic factors in moderately overweight adults. Arterioscler. Thromb 13, 162–169. [PubMed: 8427853]
50. Yuet KP, Doma MK, Ngo JT, Sweredoski MJ, Graham RLJ, Moradian A, Hess S, Schuman EM, Sternberg PW, and Tirrell DA (2015). Cell-specific proteomic analysis in Caenorhabditis elegans. Proc. Natl. Acad. Sci. USA 112, 2705–2710. [PubMed: 25691744]
51. Erdmann I, Marter K, Kobler O, Niehues S, Abele J, Müller A, Bussmann J, Storkebaum E, Ziv T, Thomas U, and Dieterich DC (2015). Cell-selective labelling of proteomes in Drosophila melanogaster. Nat. Commun 6, 7521. [PubMed: 26138272]
52. Yang R, Meyer AS, Droujinine IA, Udeshi ND, Hu Y, Guo J, McMahon JA, Carey DK, Xu C, Fang Q, et al. (2022). A genetic model for in vivo proximity labelling of the mammalian secretome. Open Biol 12, 220149. [PubMed: 35946312]
53. Wei W, Riley NM, Yang AC, Kim JT, Terrell SM, Li VL, Garcia-Contreras M, Bertozzi CR, and Long JZ (2021). Cell type-selective secretome profiling in vivo. Nat. Chem. Biol 17, 326–334. [PubMed: 33199915]
54. Das SK, Roberts SB, Bhapkar MV, Villareal DT, Fontana L, Martin CK, Racette SB, Fuss PJ, Kraus WE, Wong WW, et al. (2017). Body-composition changes in the Comprehensive Assessment of Long-term Effects of Reducing Intake of Energy (CALERIE)-2 study: a 2-y randomized controlled trial of calorie restriction in nonobese humans. Am. J. Clin. Nutr 105, 913–927. [PubMed: 28228420]
55. Mitchell SJ, Madrigal-Matute J, Scheibye-Knudsen M, Fang E, Aon M, González-Reyes JA, Cortassa S, Kaushik S, Gonzalez-Freire M, Patel B, et al. (2016). Effects of Sex, Strain, and Energy Intake on Hallmarks of Aging in Mice. Cell Metab 23, 1093–1112. [PubMed: 27304509]

56. Mattison JA, Colman RJ, Beasley TM, Allison DB, Kemnitz JW, Roth GS, Ingram DK, Weindruch R, de Cabo R, and Anderson RM (2017). Caloric restriction improves health and survival of rhesus monkeys. Nat. Commun 8, 14063. [PubMed: 28094793]
57. Miles LA, Baik N, Lighvani S, Khaldoyanidi S, Varki NM, Bai H, Mueller BM, and Parmer RJ (2017). Deficiency of plasminogen receptor, Plg-RKT , causes defects in plasminogen binding and inflammatory macrophage recruitment in vivo. J. Thromb. Haemost 15, 155–162. [PubMed: 27714956]
58. Liu L, Cheung TH, Charville GW, and Rando TA (2015). Isolation of skeletal muscle stem cells by fluorescence-activated cell sorting. Nat. Protoc 10, 1612–1624. [PubMed: 26401916]
59. Ravussin E, Redman LM, Rochon J, Das SK, Fontana L, Kraus WE, Romashkan S, Williamson DA, Meydani SN, Villareal DT, et al. (2015). A 2-Year Randomized Controlled Trial of Human Caloric Restriction: Feasibility and Effects on Predictors of Health Span and Longevity. J. Gerontol. A Biol. Sci. Med. Sci 70, 1097–1104. [PubMed: 26187233]
60. Bareja A, Hodgkinson CP, Soderblom E, Waitt G, and Dzau VJ (2018). The proximity-labeling technique BioID identifies sorting nexin 6 as a member of the insulin-like growth factor 1 (IGF1)-IGF1 receptor pathway. J. Biol. Chem 293, 6449–6459. [PubMed: 29530981]
61. White JP, Baltgalvis KA, Sato S, Wilson LB, and Carson JA (2009). Effect of nandrolone decanoate administration on recovery from bupivacaine-induced muscle injury. J. Appl. Physiol 107, 1420–1430. [PubMed: 19745189]
62. Baht GS, Bareja A, Lee DE, Rao RR, Huang R, Huebner JL, Bartlett DB, Hart CR, Gibson JR, Lanza IR, et al. (2020). Meteorin-like facilitates skeletal muscle repair through a Stat3/IGF-1 mechanism. Nat. Metab 2, 278–289. [PubMed: 32694780]
63. Mehus AA, Anderson RH, and Roux KJ (2016). BioID Identification of Lamin-Associated Proteins. Methods Enzymol 569, 3–22. [PubMed: 26778550]
64. Fortin JP, Triche TJ Jr., and Hansen KD (2017). Preprocessing, normalization and integration of the Illumina HumanMethylationEPIC array with minfi. Bioinformatics 33, 558–560. [PubMed: 28035024]
65. Salas LA, Koestler DC, Butler RA, Hansen HM, Wiencke JK, Kelsey KT, and Christensen BC (2018). An optimized library for reference-based deconvolution of whole-blood biospecimens assayed using the Illumina HumanMethylationEPIC BeadArray. Genome Biol 19, 64. [PubMed: 29843789]
66. Civitarese AE, Carling S, Heilbronn LK, Hulver MH, Ukropcova B, Deutsch WA, Smith SR, and Ravussin E; CALERIE Pennington Team (2007). Calorie restriction increases muscle mitochondrial biogenesis in healthy humans. PLoS Med 4, e76. [PubMed: 17341128]
67. Liao Y, Smyth GK, and Shi W (2014). featureCounts: an efficient general purpose program for assigning sequence reads to genomic features. Bioinformatics 30, 923–930. [PubMed: 24227677]
68. Liao Y, Smyth GK, and Shi W (2019). The R package Rsubread is easier, faster, cheaper and better for alignment and quantification of RNA sequencing reads. Nucleic Acids Res 47, e47. [PubMed: 30783653]
69. Robinson MD, McCarthy DJ, and Smyth GK (2010). edgeR: a Bioconductor package for differential expression analysis of digital gene expression data. Bioinformatics 26, 139–140. [PubMed: 19910308]
70. Kraus WE, Bhapkar M, Huffman KM, Pieper CF, Krupa Das S, Redman LM, Villareal DT, Rochon J, Roberts SB, Ravussin E, et al. (2019). 2 years of calorie restriction and cardiometabolic risk (CALERIE): exploratory outcomes of a multicentre, phase 2, randomised controlled trial. Lancet Diabetes Endocrinol 7, 673–683. [PubMed: 31303390]
71. Bates D, Mächler M, Bolker B, and Walker S (2015). Fitting Linear Mixed-Effects Models Using lme4. J. Stat. Softw 67, 1–48.

Highlights

- Short-term caloric restriction (CR) drastically alters the liver-derived plasma proteome
- Circulating plasminogen increases with CR, which is necessary for satellite cell expansion
- During CR, plasminogen signals to the satellite cell via the plasminogen receptor Plg-R_{KT}
- Loss of Plg-R_{KT} prevents CR-induced SC expansion and associated regenerative enhancements

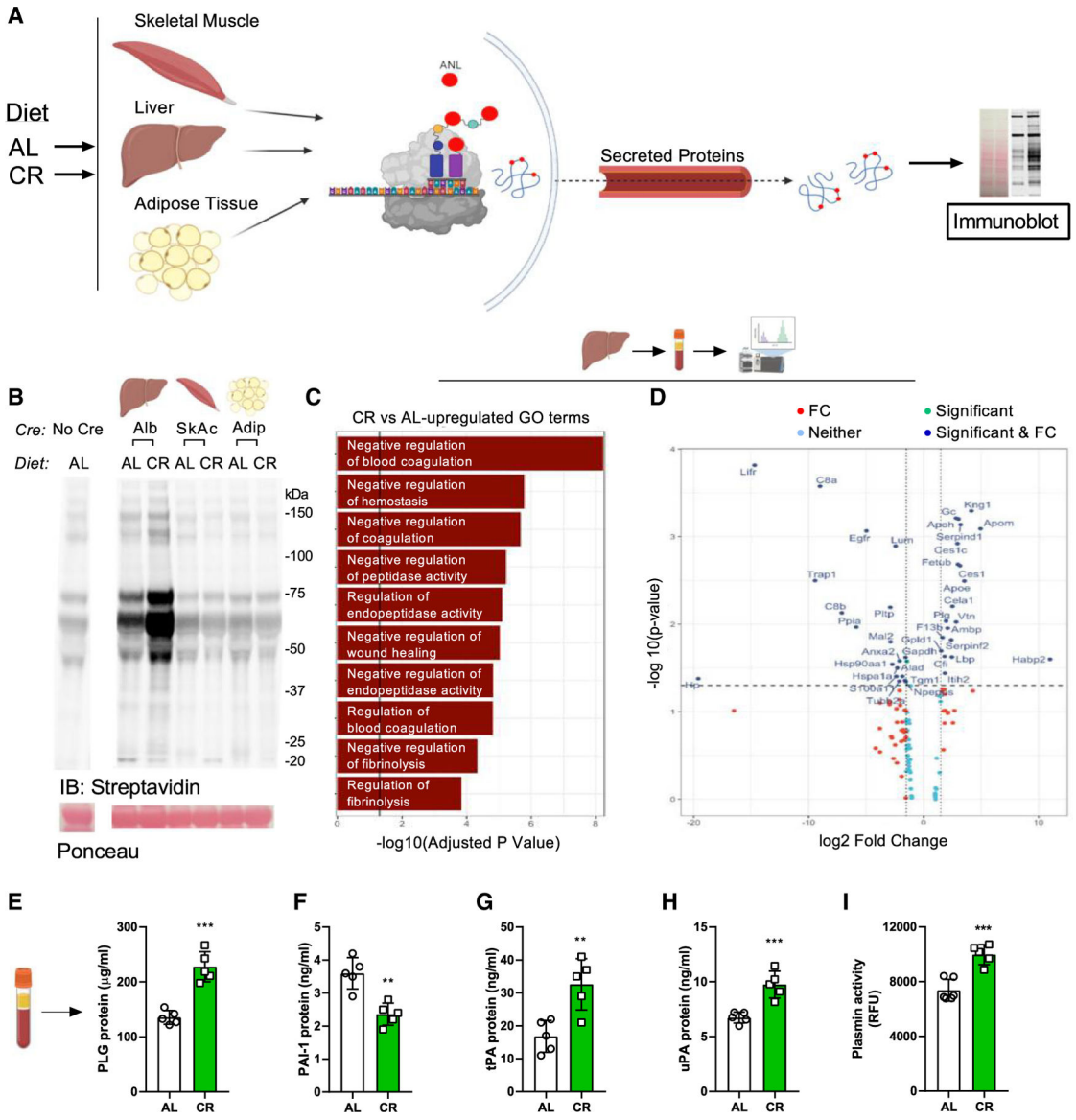

Figure 1. Proteomics analysis identifies liver-derived plasminogen secretion during short-term CR

(A) Study design using the MetRS transgenic mouse bred with muscle, adipose, and liver-specific Cre lines. Each line was put on a 40% CR or AL diet for 3 months and then given ANL to track secreted plasma proteins from their respective tissue. Plasma was collected to isolate labeled proteins and determine changes in respective protein immunoblots with streptavidin, comparing CR and AL groups.

(B) Representative immunoblot of labeled plasma protein for each tissue under the AL or CR diet.

(C) Protein ontology analysis comparing enriched biological pathways between AL and CR diets in the MetRS × Alb Cre mouse (n = 3).

(D) Volcano plot comparing differential protein abundance of labeled plasma proteins between AL and CR diets in the MetRS × Alb Cre mouse (n = 3). (E–H) Quantification

of plasma proteins (E) plasminogen, (F) PAI-1, (G) tPA, and (H) uPA in mice fed AL and CR diets for 3 months (n = 5).

(I) Plasma plasmin activity in mice fed AL or CR diets for 3 months (n = 5). Bar graphs show mean ± SE with each dot as an independent mouse. Statistical significance was tested by an unpaired Student's t test (E–I). *p < 0.05, **p < 0.01, ***p < 0.001.

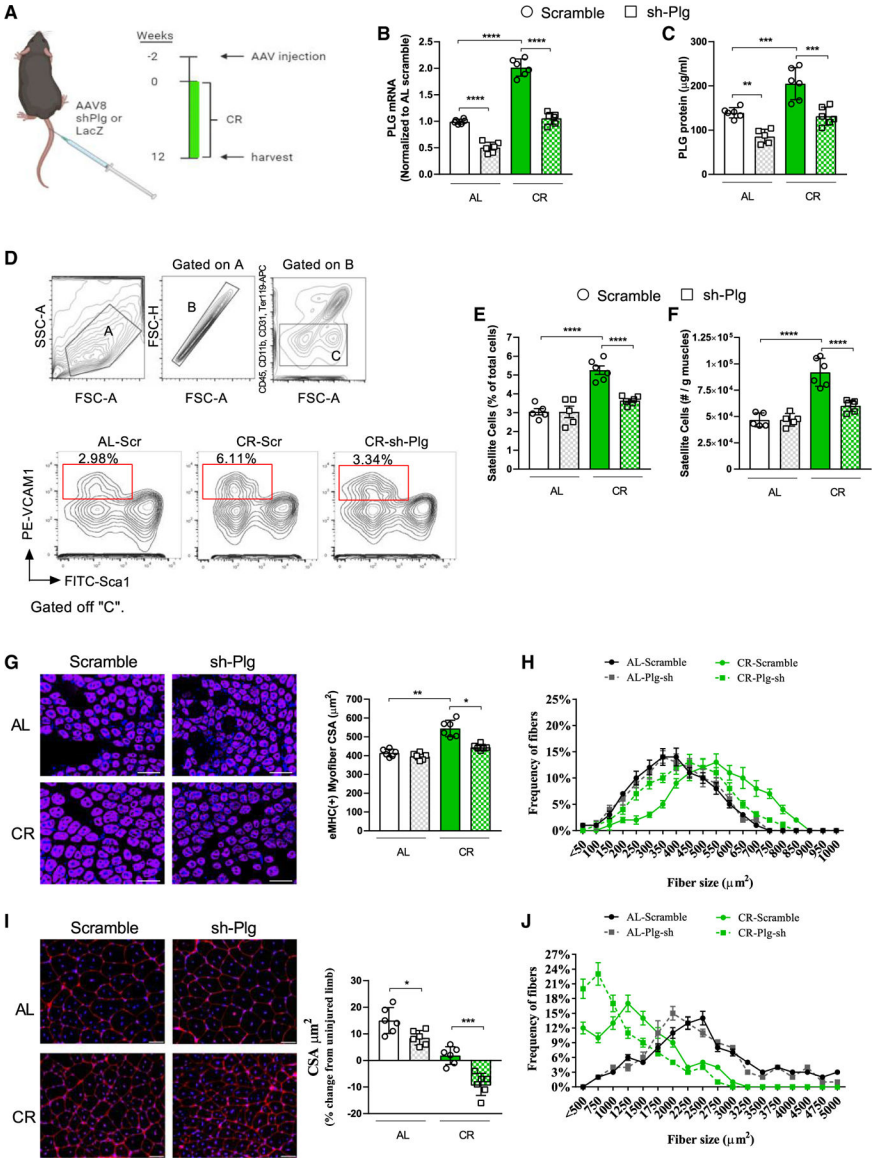

Figure 2. Knockdown of circulating plasminogen prevents satellite cell expansion during short-term CR

(A) Study design showing AAV-induced expression of sh-Plg given 2 weeks before the CR diet.

(B) Liver plasminogen gene expression with scramble and sh-Plg AAV treatment in mice on the AL or CR diet (n = 6).

(C) Circulating plasminogen protein abundance with scramble and sh-Plg AAV treatment in mice on the AL or CR diet (n = 6).

(D) Representative FACS gating strategy to isolate and quantify freshly sorted satellite cells from muscle tissue from mice fed an AL or CR diet. (E and F) Quantification of satellite cells by percentage of total cells (E) and satellite cells per gram of muscle tissue (F).

(G) Left: representative images of embryonic myosin heavy chain (eMHC) staining on muscle cross-sections 5 days after $BaCl_2$ injury. Right: quantification of eMHC(+) fiber CSA plotted as fiber size. Scale bars, 75 μm (n = 6).

(H) Frequency distribution of eMHC(+) muscle fibers across all groups.
(I) Left: representative images of muscle cross-sections stained with wheat germ agglutinin (WGA) 30 days after $BaCl_2$ injury. Right: quantification of percentage change in fiber CSA versus uninjured muscle. Scale bars, 50 μm (n = 6).
(J) Frequency distribution of muscle fiber areas across all groups. Bar graphs show mean ± SE with each dot as an independent mouse. Statistical significance was tested by a two-way ANOVA with Tukey's multiple-comparisons test (B, C, E, F, G, and I) and chi-square test (H and J). *p < 0.05, **p < 0.01, ***p < 0.001, ****p < 0.0001.

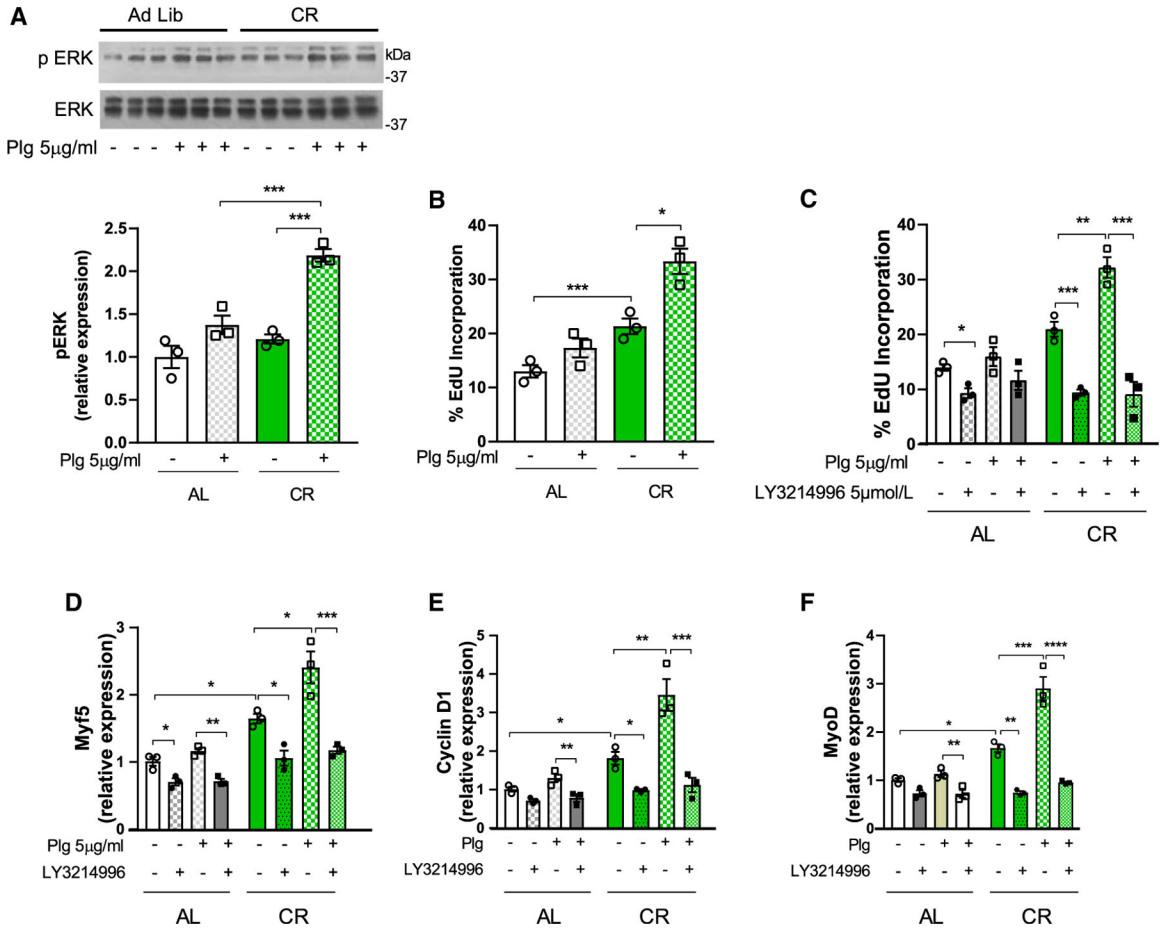

Figure 3. Plasminogen signals directly to satellite cells to activate the ERK pathway

(A) Top: immunoblot showing p-ERK and total ERK expression in cultured satellite cells after treatment (5 μg/mL, 15 min) with plasminogen or control vehicle. Cells were isolated from mice on the AL or CR diet. Bottom: quantification of relative expression (n = 3).

(B) Percent EdU (5-ethynyl-2'-deoxyuridine) incorporation in cultured satellite cells after treatment (24 h) with plasminogen (5 μg/mL) or control (DMSO) vehicle. Cells were isolated from mice on the AL or CR diet (n = 3).

(C) Percent EdU incorporation in cultured satellite cells after treatment (24 h) with vehicle control, plasminogen, and/or the ERK inhibitor LY3214996 (5 μmol/L). Cells were isolated from mice on the AL or CR diet (n = 3).

(D–F) Gene expression of satellite cell proliferative genes in cultured satellite cells after treatment (24 h) with vehicle control, plasminogen, and/or the ERK inhibitor LY3214996. Cells were isolated from mice on the AL or CR diet. Shown is quantification of (D) Myf5, (E) Cyclin D1, and (F) MyoD (n = 3).

Bar graphs show mean ± SE with each dot as an independent mouse. Statistical significance was tested by a two-way ANOVA with Tukey's multiple-comparisons test. *p < 0.05, **p < 0.01, ***p < 0.001, ****p < 0.0001.

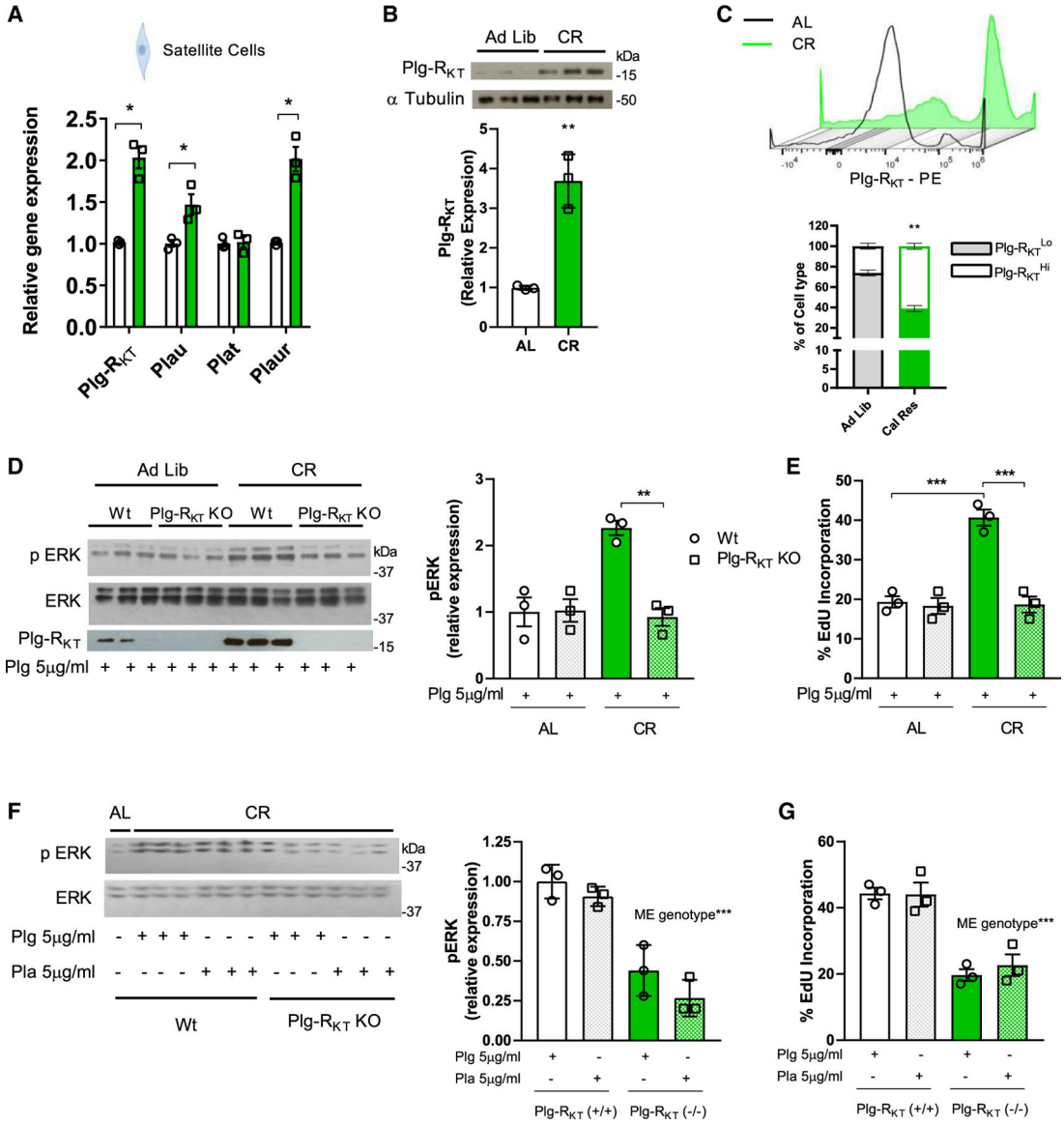

Figure 4. The plasminogen receptor Plg-RKT is increased with CR and regulates satellite cell signaling and proliferation

(A) Satellite cell gene expression of the plasminogen processing genes Plg-R_{KT}, Plau, Plat, and Plaur freshly sorted from mice fed the AL or CR diet (n = 3).

(B) Top: immunoblot showing Plg-R_{KT} protein expression in freshly sorted satellite cells isolated from mice on the AL or CR diet. Bottom: quantification of relative expression (n = 3).

(C) Top: flow plot illustrating Plg-R_{KT} expression on satellite cells isolated from mice on the AL or CR diet. Bottom: quantification of satellite cell Plg-R_{KT} intensity among AL and CR groups, displayed as percentage of cells expressing high or low Plg-R_{KT} (n = 4).

(D) Left: immunoblot showing p-ERK and total ERK and Plg-R_{KT} protein expression in cultured satellite cells after treatment (5 μg/mL, 15m) with plasminogen. Cells were isolated from wild-type or Plg-R_{KT} KO mice on the AL or CR diet. Right: quantification of relative expression (n = 3).

(E) Percent EdU incorporation in cultured satellite cells after treatment (24 h) with plasminogen. Cells were isolated from wild-type and Plg-R_{KT} KO mice on the AL or CR diet (N = 3).

(F) Left: immunoblot showing p-ERK and total ERK expression in cultured satellite cells after treatment with plasminogen (5 μg/mL, 15m) and plasmin (5 μg/mL, 15m). Cells were isolated from wild-type or Plg-R_{KT} KO mice on the AL or CR diet. Right: quantification of relative expression (n = 3). ME, main effect.

(G) Percent EdU incorporation in cultured satellite cells after treatment (24 h) with plasminogen (5 μg/mL) and plasmin (5 μg/mL). Cells were isolated from wildtype or Plg-R_{KT} KO mice on the AL or CR diet (n = 3).

Bar graphs show mean ± SE with each dot as an independent mouse. Statistical significance was tested by an unpaired Student's t test (A–C) and two-way ANOVA with Tukey's multiple-comparisons test (D–G). *$p < 0.05$, **$p < 0.01$, ***$p < 0.001$, ****$p < 0.0001$.

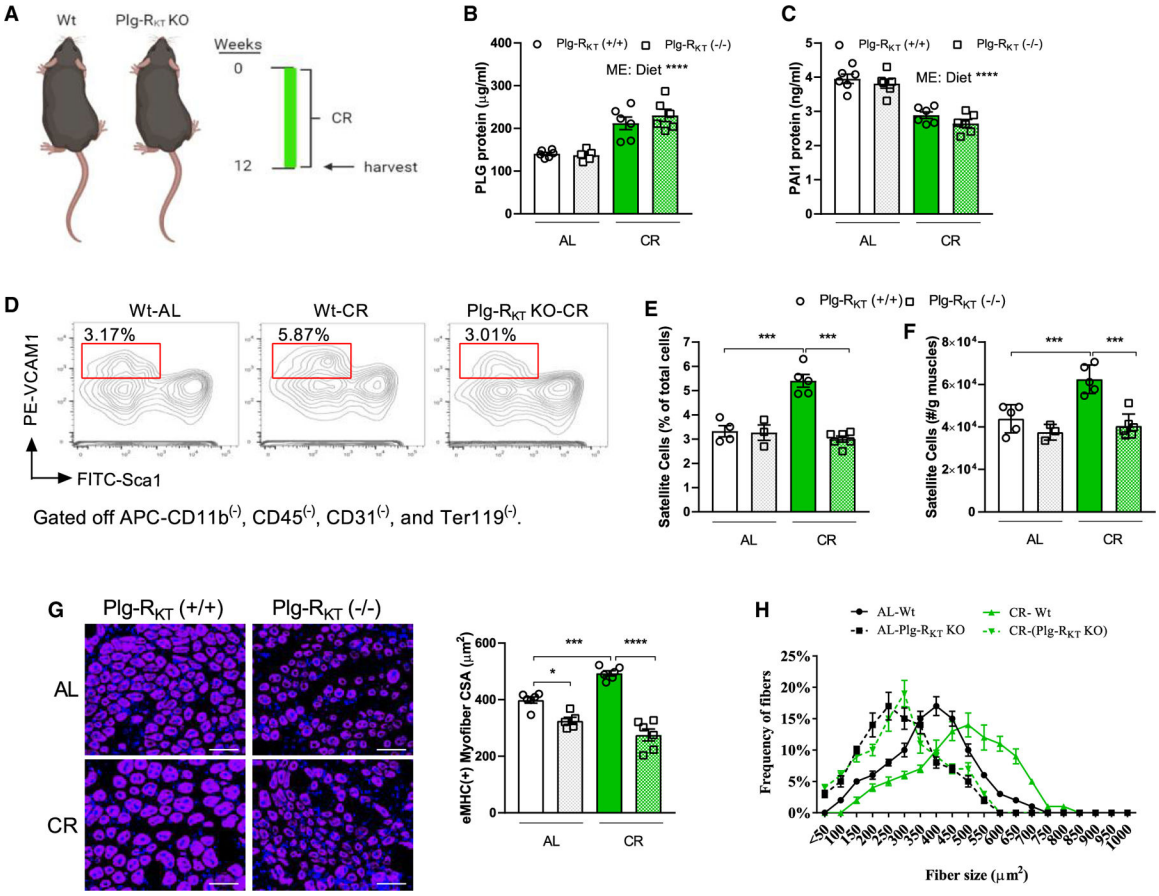

Figure 5. Loss of Plg-RKT inhibits satellite cell expansion during short-term CR

(A) Study design, showing 3 months of the CR diet in wild-type and Plg-R_{KT} KO mice.

(B and C) Circulating (B) plasminogen and (C) PAI-1 protein abundance in wild-type and Plg-R_{KT} KO mice on the AL or CR diet (n = 6).

(D) Representative FACS plots of freshly isolated satellite cells in wild-type and Plg-R_{KT} KO mice on the AL or CR diet (n = 6). (E and F) Quantification of satellite cells by percent total cells (E) and satellite cells per gram of muscle tissue (F) (n = 6).

(G) Left: representative images of eMHC staining on muscle cross-sections 5 days after $BaCl_2$ injury. Sections were taken from wild-type and Plg-R_{KT} KO mice on the AL or CR diet. Scale bars, 75 µm (n = 6). Right: quantification of eMHC(+) fiber CSA plotted as fiber size.

(H) Frequency distribution of eMHC(+) muscle fibers across all groups.

Bar graphs show mean ± SE with each dot as an independent mouse. Statistical significance was tested by a two-way ANOVA with Tukey's multiple-comparisons test (B, C, E, F, and G) and chi-square test (H). ***p < 0.001, ****p < 0.0001.

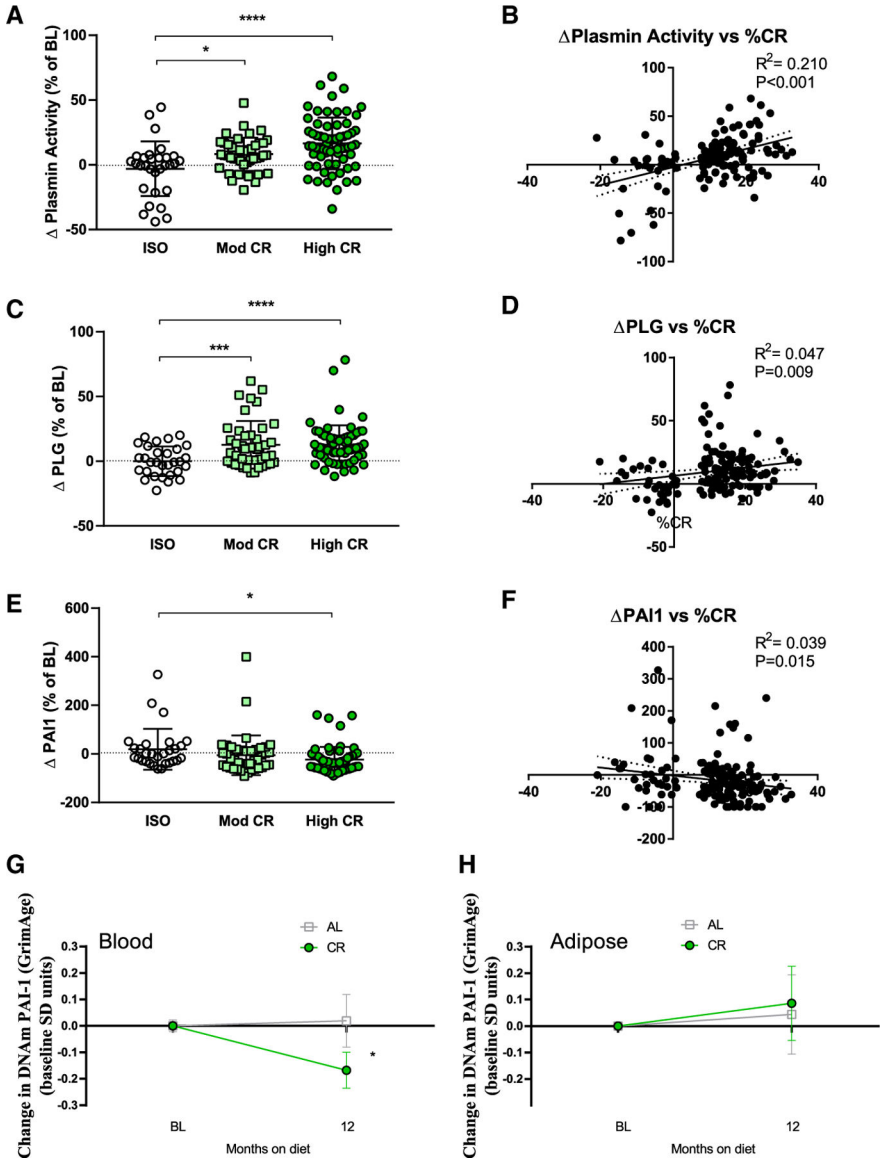

Figure 6. Validation of plasminogen activation in the CALERIE cohort

(A) Plasma plasmin activity in participants in the CALERIE cohort, stratified by percent CR. Percent CR was derived from percent change in calories consumed at the pre and 12-month time point. The delta change was calculated as percent change from baseline to 12 months.

(B) Correlation between Δplasmin activity (y axis) and % CR (x axis).

(C) Circulating plasminogen protein across CR groups, presented as % Δ from baseline.

(D) Correlation between Δ plasminogen protein (y axis) and % CR (x axis).

(E) Circulating PAI-1 protein across CR groups presented as % Δ from baseline.

(F) Correlation between ΔPAI-1 protein (y axis) and % CR (x axis). High CR group, n = 76; moderate CR group, n = 43; isocaloric group, n = 33. Error bars represent SEM.

(G and H) DNAmPAI1 levels in (G) blood and (H) adipose tissue in the CALERIE trial AL control group and CR treatment group at the 12-month followup. The y axis values

are scaled by the standard deviation of DNAmPAI1 at pre-treatment baseline. For (G): AL group, n = 65; CR group, n = 125. For (H): AL group, n = 14, CR group, n = 29. Graphs show mean ± SD with each dot as an independent subject. Statistical significance was tested by a one-way ANOVA with Tukey's multiple comparison test (A, C, and E), linear regression analysis (B, D, and F), and repeated-measures analysis of covariance (ANCOVA) implemented under mixed models (G and H). *p < 0.05, ***p < 0.001, ****p < 0.0001.

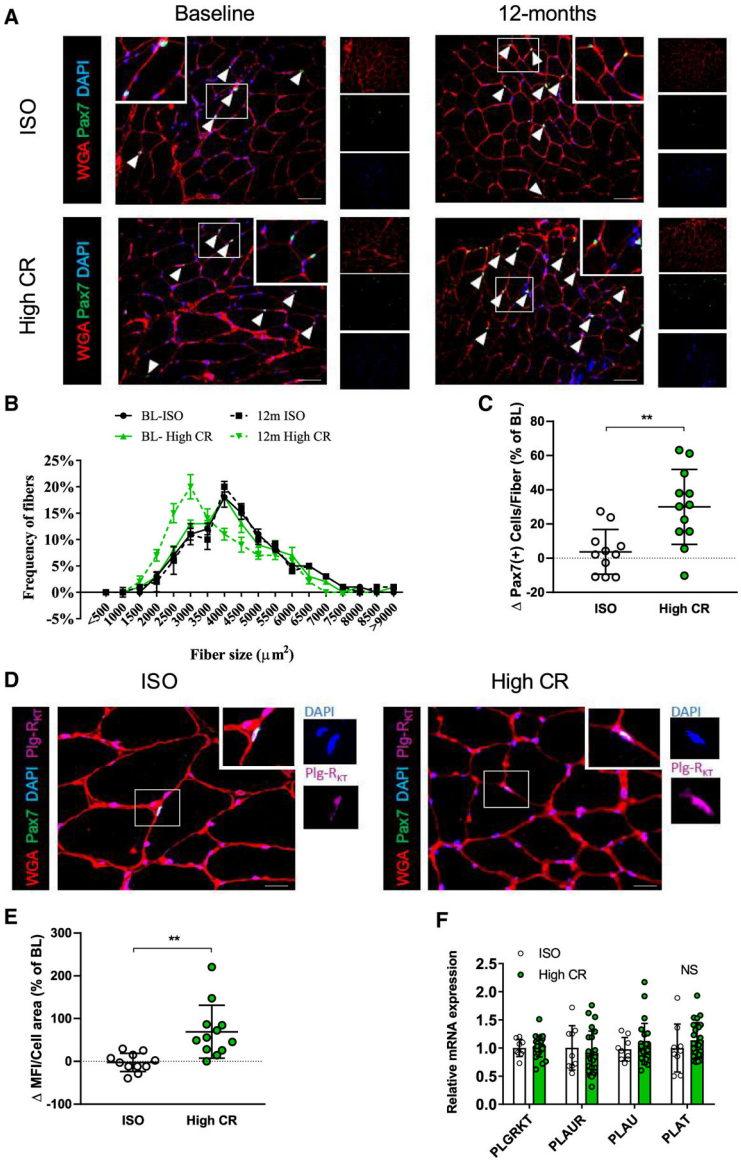

Figure 7. Human muscle analysis from the CALERIE trial shows similar effects of CR

(A) Representative images of muscle cross-sections stained with WGA, Pax7, and DAPI. Sections are from baseline biopsies and after 12 months of CR. Scale bars, 50 μm. Arrows indicate DAPI(+), Pax7(+) cells.

(B) CSA frequency distribution among baseline and 12-month time points in both CR and isocaloric groups.

(C) Percent change in Pax7-positive cells normalized to fiber number from baseline to the 12-month followup.

(D) Representative images of muscle sections stained with WGA (red), Pax7 (green), DAPI (blue), and Plg-R_{KT} (purple) across isocaloric and CR groups. The magnified inset shows a representative satellite cell with Plg-R_{KT} staining. Scale bars, 100 μm.

(E) Percent change of satellite cell mean fluorescence intensity (MFI) of Plg-R_{KT} staining normalized to satellite cell area from baseline to the 12-month followup.

(A–E) ISO group, n = 11; high CR group, n = 12.

(F) Whole-muscle mRNA expression of plasminogen processing genes after 12 months of isocaloric or CR diet. Data were generated from muscle biopsies taking in the CALERIE trial. Isocaloric, n = 9; high CR, n = 24. Graphs and bar graphs show mean ± SE (B) and ±SD (C, E, and F) with each dot as an independent subject. Statistical significance was tested by chi-square analysis (B) and an unpaired Student's t test (C, E, and F). **$p < 0.01$.

KEY RESOURCES TABLE

REAGENT or RESOURCE	SOURCE	IDENTIFIER
Antibodies		
Anti-p44/42 MAPK (Erk 1/2)	Cell Signaling Technology	Cat# 9102S; RRID: AB_330744
Anti-P-p44/42 MAPK (Erk 1/2)	Cell Signaling Technology	Cat# 9101S; RRID: AB_331646
Anti-alpha/beta-Tubulin	Cell Signaling Technology	Cat# 2148S; RRID: AB_2288042
IRDye 800 CW Streptavidin	LI-COR	Cat# 926-32230
IRDye 800 CW Goat anti-Rabbit	LI-COR	Cat# 926-32211; RRID: AB_621843
Anti-Pax7	Developmental Studies Hybridoma Bank, U of Iowa	PAX7; RRID: AB_2299243
Anti-Plg-R_{KT}	ThermoFisher	Cat#PA5-98932; RRID: AB_2813545
Alexa Fluor 647	Invitrogen	Cat#A32733; RRID: AB_2633282
Anti-eMHC_BF-G6	Developmental Studies Hybridoma Bank, U of Iowa	Cat#BF-G6; RRID: AB_10571455
Anti-GFP	Cell Signaling Technology	Cat#2555; RRID: AB_10692764
APC-CD45	Biolegend	Cat#157605: RRID: AB_2876537
APC-CD11b	Biolegend	Cat#101211; RRID: AB_312794
APC-CD31	Biolegend	Cat#102410; RRID: AB_312904
APC-Ter119	Biolegend	Cat#116212; RRID: AB_313713
FITC-Sca1/Ly6a	Biolegend	Cat#108105; RRID: AB_313342
PE-VCAM1/CD106	Biolegend	Cat#105713; RRID: AB_1134164
Anti-rabbit PE secondary	ThermoFisher	Cat#P-2771MP; RRID: AB_2539845
Anti-rabbit Alexa Flour™ 647 Plus secondary	ThermoFisher	Cat#A32733; RRID: AB_2633282
Anti-mouse FITC secondary	ThermoFisher	Cat#F-2765; RRID: AB_2536525
Anti-rabbit IgG, HRP-linked Antibody	Cell Signaling Technology	Cat#7074; RRID: AB_2099233
Hyperfilm™ ECL™	Sigma-Aldrich	Cat#GE28-9068-36
Biological samples		
CALERIE™ plasma	CALERIE™ Bio repository	https://calerie.duke.edu/sites/default/files/2022-05/phase2_protocol.pdf
CALERIE™ muscle biopsies	CALERIE™ Bio repository	https://calerie.duke.edu/sites/default/files/2022-05/phase2_protocol.pdf
CALERIE™ adipose tissue	CALERIE™ Bio repository	https://calerie.duke.edu/sites/default/files/2022-05/phase2_protocol.pdf
Chemicals, peptides, and recombinant proteins		
DAPI	ThermoFisher	Cat#62248
EdU	Sigma-Aldrich	Cat# 900584
WGA 555	ThermoFisher	Cat#W32464
Biotin-PEG4-Alkyne	Click Chemistry Tools	Cat# TA105
6-Azido-L-lysine-HCl	Jena Bioscience	Cat# CLK-AA009
Trizma hydrochloride solution	Sigma-Aldrich	Cat# T2194
Sodium dodecyl sulfate	Sigma-Aldrich	Cat# 436143

REAGENT or RESOURCE	SOURCE	IDENTIFIER
Triton X-100	Sigma-Aldrich	Cat# 11332481001
Bovine Serum Albumin	Sigma-Aldrich	Cat# 2153
Dimethyl sulfoxide	Sigma-Aldrich	Cat# D8418
Protease Inhibitor Cocktail	Sigma-Aldrich	Cat# P8340
PhosSTOP	Sigma-Aldrich	Cat# 04906837001
2-Mercaptoethanol	Sigma-Aldrich	Cat# M6250
Ponceau S solution	Sigma-Aldrich	Cat# P7170
NuPAGE MOPS SDS Running Buffer (20X)	Thermo Fisher Scientific	Cat# NP0001
NuPAGE MES SDS Running Buffer (20X)	Thermo Fisher Scientific	Cat# NP0002
NuPAGE Transfer Buffer (20X)	Thermo Fisher Scientific	Cat# NP00061
Gibco PBS, pH 7.4	Thermo Fisher Scientific	Cat# 10010023
UltraPure Dnase/Rnase-Free Distilled Water	Thermo Fisher Scientific	Cat# 10977015
TRIzol Reagent	Thermo Fisher Scientific	Cat# 15596018
PowerUp SYBR Green Master Mix	Thermo Fisher Scientific	Cat# A25742
Dynabeads MyOne Streptavidin C1	Thermo Fisher Scientific	Cat# 65001
LY3214996	Cayman Chemicals	Cat#27936
recombinant Plasminogen protein	abcam	Cat#200264
recombinant Plasmin protein	abcam	Cat#90928
Critical commercial assays		
RC DC Protein Assay Kit II	Bio-Rad	Cat# 5000122
High-Capacity cDNA Reverse Transcription Kit	Thermo Fisher Scientific	Cat# 4368813
Click-&-Go Protein Reaction Buffer Kit	Click Chemistry Tools	Cat# 1262
Plasmin Activity Assay Kit (Fluorometric)	abcam	Cat# ab204728
Plasminogen ELISA (mouse)	abcam	Cat# ab198511
Plasminogen ELISA (human)	abcam	Cat# ab108893
PAI-1 (SERPINE1) (mouse)	abcam	Cat# ab197752
PAI-1 (SERPINE1) (human)	abcam	Cat# ab269373
uPA (mouse)	abcam	Cat# ab245727
tPA (mouse)	abcam	Cat# ab233615
Deposited data		
Proteomics	This paper	ProteomeXchange with identifier PXD043644
CALERIE™ Muscle RNAseq	Das et al.[41]	https://doi.org/10.1111/acel.13963
Experimental models: Organisms/strains		
Mouse: C57BL6/J	Jackson Laboratories	Cat# 000664
Mouse: C57BL/6-*Gt(ROSA)26Sortm1(CAG-GFP,-Mars*L274G)Esm*/J	Jackson Laboratories	Cat# 028071
Mouse: B6.Cg-*Speer6-ps1*$^{Tg(Alb\text{-}cre)21Mgn}$/J	Jackson Laboratories	Cat# 003574
Mouse: B6.FVB-Tg(Adipoq-cre)1Evdr/J	Jackson Laboratories	Cat# 028020
Mouse: B6.Cg-Tg(ACTA1-cre)79Jme/J	Jackson Laboratories	Cat# 006149

REAGENT or RESOURCE	SOURCE	IDENTIFIER
Oligonucleotides		
See Table S2	This paper	N/A
Recombinant DNA		
AAV8-U6-PLG-shRNA	Vector Biosystems	Cat# shAAV-268877
AAV8-GFP-U6-shRNA	Vector Biosystems	Custume order
Software and algorithms		
R(v4.0.5)	R Core Team	https://www.r-project.org/
RStudio(v1.4.1106)	RStudio	https://www.rstudio.com/
GraphPad Prism 6	GraphPad Software	https://www.graphpad.com/scientific-software/prism/
ImageJ	ImageJ	https://ImageJ.nih.gov/ij
FlowJo	FlowJo	https://www.flojo.com/